1

An Introduction to Noble Metal-Based Composite Nanomaterials

1.1 Materials at Nanometer Scales

Materials including semiconductors, metals, and oxides at nanometer scales, in terms of nanomaterials, nanoparticles, or nanocrystals with controlled sizes/morphologies, have garnered a great deal of research interest due to their immense potential for various applications, e.g. catalysis and photonics [1–19]. Owing to the quantum confinement effect and/or the large surface-to-volume ratio, the physical and chemical properties of materials at nanometer scale are usually dependent on size and shape [4, 5, 12–14, 20–25]. One typical example to indicate the size influence on the chemical property of nanometer materials is the catalytic reduction of *p*-nitrophenol to *p*-aminophenol over gold (Au) nanoparticles stabilized by cetyltrimethyl ammonium bromide (CTAB) with average sizes in the range of 3.5–56 nm. The results suggest that the activity of the CTAB-stabilized Au nanoparticles is neither very efficient for the smallest particles (3.5 nm) nor for the larger ones (28 and 56 nm). Instead, it turns out that the CTAB-stabilized Au nanoparticles of an intermediate size (13 nm) are the most active ones for the catalytic reduction of *p*-nitrophenol to *p*-aminophenol [26]. In addition, for noble metal nanoparticles with different shapes, they could display different activities for the same catalytic reaction due to their different crystallographic surfaces [2, 3, 5, 12–14, 27, 28]. In other words, noble metal nanoparticles with different shapes often display quite different catalytic behaviors [12, 13]. For instance, Wang and coworkers demonstrated that the monodispersed Pt nanoparticles with controlled sizes of 3–7 nm and shapes of polyhedron, truncated cube, or cube are active catalysts for the oxygen reduction reaction (ORR) in acidic medium. However, the measured current density for 7-nm Pt nanocubes is four times that of 3-nm polyhedral (or 5-nm truncated cubic) Pt nanoparticles, manifesting a significant effect of particle shape on the oxygen reduction [8].

We are currently witnessing the impressive successes in preparation of materials at nanometer scale. Over the past decades, a vast number of wet-chemistry approaches, including the reduction of appropriate precursors in solution phases [14, 29–34], in microemulsions [35], or in sol–gel processes [36], have been developed to obtain various nanoparticles with well-defined sizes and shapes.

Noble Metal-Based Nanocomposites: Preparation and Applications, First Edition. Jun Yang.

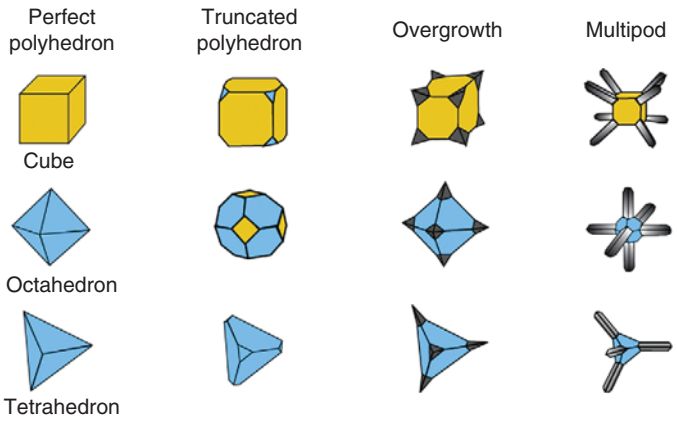

Figure 1.1 Schematic illustration of different shapes of Pt nanocrystals derived from conventional single-crystal polyhedrons enclosed by the low-index planes {100} and {111}. The first column represents the perfect polyhedrons, while the second column contains the truncated forms of the perfect polyhedrons. The third and fourth columns compromise the overgrown nanostructures and highly branched nanostructures grown from the corners of the perfect polyhedrons, respectively. The yellow and blue colors represent the {100} and {111} facets, respectively. Source: Chen et al. 2009 [12]. Adapted with permission of Elsevier.

Further, the size/shape control of the nanoparticles could also be achieved through control of the nucleation and growth by varying the synthetic parameters, including the activity of the reducing agents, the type and concentration of the precursors, and the nature and amount of surfactants or protective reagents [33, 37–43]. As an important noble metal used in a wide variety of catalytic applications, single-crystalline platinum (Pt) nanoparticles with diverse shapes, as summarized in Figure 1.1, have been synthesized in the presence of a capping agent through reducing a Pt precursor, decomposing an organometallic complex, or combining these two routes such as hydrogenated decomposition of platinum(II) acetylacetonate ($Pt(acac)_2$) [12].

Another common strategy used to generate nanomaterials with controlled sizes/shapes is the seed-mediated growth method. The core particle in this case is overlaid with a single shell of another material to realize the preparation of nanoparticles with desired sizes/shapes [44–50]. The core of the nanoparticles could be subsequently removed by calcination or with a solvent for further tailoring of the particle structures [51–57]. As schematically shown in Figure 1.2, in a typical example, core–shell silver (Ag)–noble metals including ruthenium (Ru), rhodium (Rh), platinum (Pt), osmium (Os), iridium (Ir), and their alloys or core–shell–shell nanoparticles with Ag residing in the inner shell region were firstly synthesized in an organic solvent. The Ag was then extracted from the core or the inner shell by an aqueous solution of bis(*p*-sulfonatophenyl)phenylphosphine, which binds strongly with Ag atoms or Ag^+ ions to allow the complete removal of the Ag component, leaving behind an organosol of hollow- or cage-bell-structured noble metal nanoparticles [53].

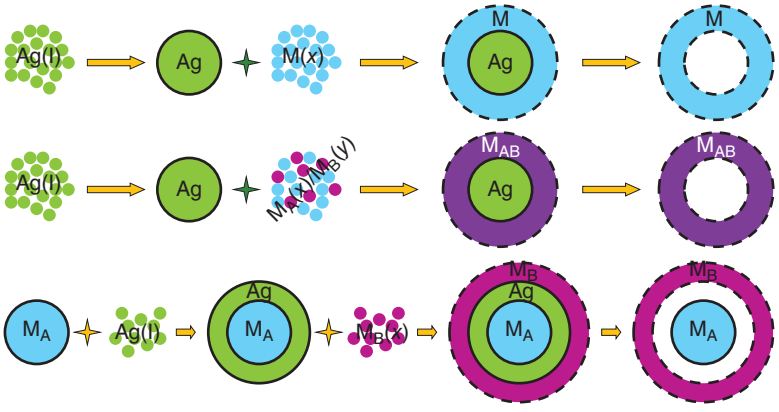

Figure 1.2 Schematic illustration to show the synthesis of noble metal nanomaterials with hollow or cage-bell structure based on the inside-out diffusion of Ag in core–shell nanoparticles with Ag residing in the core or inner shell region. Source: Liu et al. 2012 [53]. Adapted with permission of American Chemical Society.

1.2 Emergence of Composite Nanomaterials

After close to decades of intense effort in determining dominant experimental conditions, e.g. suitable precursors, templates, stabilizer molecules, relative concentration ratios, reaction media, and temperature, many nanoparticles can now be produced with fairly good control of sizes and shapes [58–64]. A number of nanoparticle geometries such as wires [65–70], rods [71–77], cubes [66, 78, 79], stars [80–83], disks [84–86], dendrites [87–94], and prisms [95, 96] can be routinely synthesized by solution chemistry methods in polar and nonpolar environments. Following the extensive progress in synthetic control achieved for nanoparticles of metals, semiconductors, and oxides, naturally, there is an increased interest in producing more sophisticated nanostructures because of the promise of tunable properties for a new generation of technology-driven applications in catalysis [97–100], chemical and biological sensing [101–105], and optics [100, 106, 107]. The increase in degree of complexity may mean increase in functionalities. As an example, the core–shell nanoparticles, in which an additional inorganic material is uniformly grown around a nanocrystal core, can be used to enhance the robustness and fluorescence efficiency of a semiconductor core [108–112], to tailor the magnetic properties of the overall particle [113, 114], and also to provide a surface to which molecules can attach easily [115].

After remarkable successes in synthesizing more conventional hybrid nanomaterials, which are featured by their combination of same type of materials, e.g. core–shell [44, 116–121], alloy [122–135], and bimetallic heterostructures with controlled dimensions and intriguing morphologies [45, 83, 90, 94, 136–141], there has been increasing interest devoted toward the development of composite nanomaterials (also called hybrid nanoparticles) that consist of different classes of materials with intimate contacts [142–161]. The lure of these composite nanostructures is that they combine disparate materials with distinctly different

physical and chemical properties onto a single nanosystem, thus providing a powerful approach for the bottom-up design of novel architectures. Beyond the fundamental development in synthesis, the interest in nanocomposites arises from their combined and synergistic properties exceeding the functionality of the individual components, which yield a unique hybrid platform with tunable optical properties [162–176], enhanced photocatalytic activities [177–187], ultrafast carrier dynamics [188–195], and photothermal therapy or cell destruction functions [196–198]. Furthermore, the interactions among their different domains can greatly improve the overall application performance of the nanocomposites. These ideas are well demonstrated by the application of metal-based nanocomposites in photocatalysis. Upon ideal combination, the solid-state interfaces among different domains in the nanocomposites can assist quick transfer of the photogenerated charge carriers from one to the other; and can delocalize the photoelectrons over the excited states of both metal and semiconductor or oxide, which in turn hinders carrier recombination, offering a better opportunity for their utilization in activating the chemical reactions [147, 156, 177, 181, 199, 200]. Further, these composite materials also provide various combinations of facets on their surfaces, which can give rise to more chances for the substrate molecules getting adsorbed [147, 201, 202]. These advantages make these metal-based nanocomposites more efficient photocatalysts than the only-metal or semiconductor/oxide catalysts. For example, the metal ingredients in semiconductor–metal nanocomposites can enhance both the photocatalytic and light-harvesting efficiencies of semiconductors by improving the charge separation and by increasing the light absorption [203–205]. In addition, as presented by Talapin et al., contrary to the n-type lead sulfide (PbS) semiconductor, core–shell-structured Au–PbS nanocomposites exhibit strong p-type gate effects due to the intraparticle charge transfer between Au core and PbS shell regions. The energy-level alignment of PbS and Au is favorable for the electron transfer from the highest occupied $1S_h$ quantum confined state of the PbS shell to the Au core, which is something like the injection of mobile holes into the PbS shell [206].

The early studies on noble metal-based nanocomposites involve the deposition or doping of different noble metals (e.g. Au, Ag, and Pt) in titanium dioxide (TiO_2) powders for photocatalytic applications [180, 207–213]. In these structures, the metal domain induces the charge equilibrium in photoexcited TiO_2 substrates to affect the energetics of the nanocomposites by shifting the Fermi level to more negative potentials. The shift in Fermi level is indicative of improved charge separation in TiO_2–noble metal systems, and is effective in enhancing the efficiency of photocatalysis [177, 178, 214, 215].

As shown in Figure 1.3, the syntheses for most of the noble metal-based nanocomposites were achieved after the year 2000. Indeed, only within the past two decades have wet chemistry methods blossomed and become a powerful approach toward the synthesis of composite nanomaterials [147, 150, 154, 156, 159–161]. In 2004, the Banin group at the Hebrew University of Jerusalem, Israel, made a major breakthrough in fabricating semiconductor–metal nanocomposites [216]. They demonstrated a solution-based synthesis for nanohybrids via the selective growth of Au tips

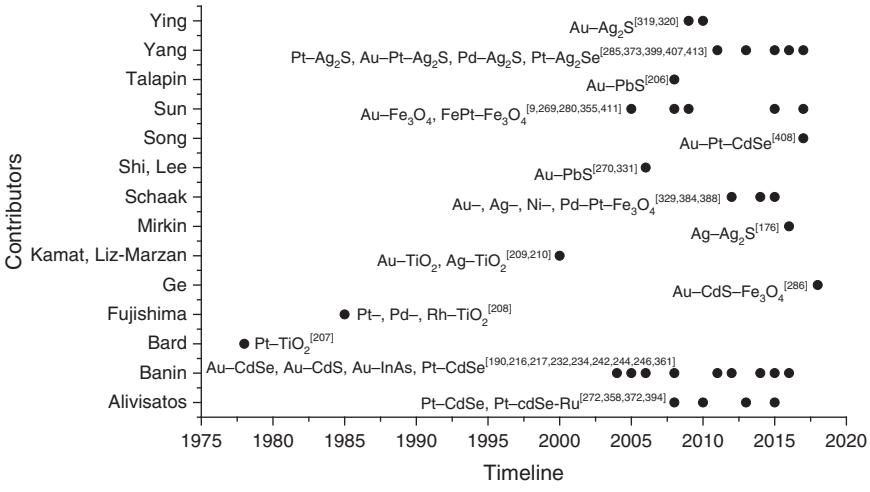

Figure 1.3 The main milestones in wet chemistry-based syntheses of noble metal-based composite nanomaterials.

on the apexes of hexagonal-phase cadmium selenide (CdSe) nanorods at room temperature. The novel nanostructures display modified optical properties due to the strong coupling between the Au and semiconductor domains. The Au tips show increased conductivity, as well as selective chemical affinity for forming self-assembled chains of rods. The architecture of these composite nanostructures is qualitatively analogous to bifunctional molecules such as dithiols, which provide two-sided chemical connectivity for self-assembly and for electrical devices, and contacting points for colloidal nanorods and tetrapods. The researchers in the Banin group later reported the synthesis of asymmetric semiconductor–noble metal heterostructures, whereby Au is grown on one side of the CdSe nanocrystalline rods and dots. Theoretical modeling and experimental analysis show that the one-sided nanocomposites are transformed from the two-sided architectures through a ripening process [217]. Subsequently, a large number of wet chemistry-based approaches were developed for the synthesis of semiconductor or metal oxide–noble metal nanocomposites, e.g. ZnO–Ag [218–224], ZnO–Au [198, 225–230], ZnO–Au–Ni [231], CdS–Au [167, 168, 192, 195, 232–249], InAs–Au [250, 251], TiO_2–Ag [252–256], TiO_2–Au [257–267], Fe_3O_4–Au [268–280], α-Fe_2O_3–Au [281, 282], Fe_3O_4–Ag [283–285], VO_2–Au [286], MnO–Au [287, 288], SiO_2–Au [170, 289, 290], CuO–Ag [187, 291], Cu_2O–Ag [172], Cu_2O–Au [292–294], CdO–Au [295], In_2O_3–Au/Ag [173, 296], $CoFe_2O_4$–Ag [297], $AgGaO_2$–Ag [298], Bi_2S_3–Au [299], CdSe–Au [165, 201, 300–312], CdTe–Au [313], CdSe–Ag [314], Ag_2S–Au [163, 315–317], Ag_2S–Ag [169, 171, 176, 318–321], AgBr–Ag [322, 323], Cu_2S–Au [324, 325], $Cu_{2-x}Se$–Au [326], PbS–Au [269, 327–329], PbSe–Au [330], PbTe–Au [331], SnS–Au [332], ZnS–Au [333–337], ZnSe [338], $CuInS_2$–Au [339], Cu_2ZnSnS_4–Au [340, 341], Si–Au [175, 197, 342, 343], and Pt, Pd, or other noble metal-based composite nanosystems [344–412], by

anisotropic or epitaxial growth of noble metals on various semiconductors/metal oxides or vice versa through reduction, physical deposition, or photochemistry.

We are interfacing a number of forefront research areas in this period of technology development. The invention and development in characterization and measurement techniques such as high-resolution transmission electron microscopy (HRTEM) offer the opportunity to study in great detail and manipulate the nanostructures or nanomaterials often down to the atomic level, which enables us to establish the synthesis–structure–performance relationship and further direct the design of new materials with the desired performance. Noble metal-based composite nanomaterials, which represent a powerful paradigm for bottom-up construction of advanced materials, have emerged in the past decade, and their progress is expected to further continue and intensify in the coming years. The nanocomposites in their constituents are not new, and they are the combination of existing materials and our synthetic capability to manipulate at nanometer or atomic scale, which makes the composite nanomaterials so compelling from the scientific viewpoint.

1.3 General Concepts in Wet Chemistry Synthesis of Composite Nanomaterials

The understanding of the formation mechanism accounting for monodispersed nanoparticles is necessary because it is helpful to develop improved synthetic methods that can be universally applicable to various kinds of metal, semiconductor, and oxide materials.

For single materials, the study on preparing uniform colloidal particles could be dated back to the 1940s. LaMer and Dinegar proposed the concept of "burst nucleation" through investigating the preparation of a variety of oil aerosols and sulfur hydrosols [14, 413, 414]. In this process, they divided the formation of colloidal particles into three stages (Figure 1.4), and assumed that many nuclei are generated at the same time, and then these nuclei start to grow without the need for additional nucleation. Because all of the particles are nucleated almost simultaneously, their growth histories are nearly the same. This is the essence of the "burst-nucleation" process, which makes it possible to control the size distribution of the ensemble of particles as a whole during the process of growth. Otherwise, if the nucleation process also occurs during the formation of particles, the growth histories of the particles would differ largely from one another, and would consequently make a great difference to the size distribution.

In the "burst-nucleation" theory, it is necessary to induce a single nucleation event and prevent additional nucleation during the subsequent growth process for the preparation of highly uniform colloidal solution. This synthetic strategy, often referred to as "separation of nucleation and growth" has been extensively used to synthesize monodispersed semiconductor nanoparticles, e.g. CdSe and InAs [415, 416]. The seed-mediated growth method is the most apparent case for the separation of nucleation and growth, wherein nucleation is physically separated from growth using preformed nanoparticles as seed nuclei. This method

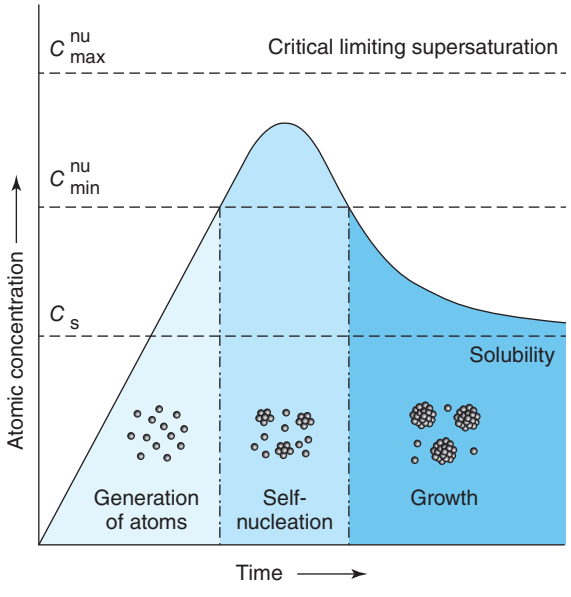

Figure 1.4 Plot of atomic concentration against time, illustrating the generation of atoms, nucleation, and subsequent growth. Source: Adapted from Xia et al. [14] and Carbone and Cozzoli [413].

utilizes heterogeneous nucleation to suppress the formation of additional nuclei by homogeneous nucleation [417–420]. In this method, the preformed nuclei, which have to be uniform in size, are introduced into the reaction solution and then the monomers, which refer to the highly reactive species generated as the synthesis is activated, are supplied to precipitate on the surface of the existing nuclei. The monomer concentration is kept low during growth to suppress homogeneous nucleation. Seed-mediated growth is further divided into two categories: the synthesis of homogeneous particles [417, 420] and the production of heterogeneous structures, such as core@shell structures [418, 419].

In the growth stage of nanoparticles, the agglomeration or aggregation of small particles is inevitable in the absence of stabilizers as the thermodynamics favor the minimization of the surface/volume ratio. Alternatively, the surface energy can be well controlled by absorbing some capping agents [14, 21, 421]. The capping agents play several key roles during the synthesis of the nanoparticles. Indeed, they form complexes with the monomers, thereby tuning their reactivity, while they simultaneously participate in an adsorption/desorption dynamics at the surface of the growing clusters, which prevents them from aggregation and uncontrolled growth [143]. In this sense, knowledge and studies in surface science would be helpful in designing nanoparticles with desired sizes/shapes, which might be featured with specific facets. In addition, both thermodynamics and kinetics can affect the growth of metal nanoparticles. Compared with the growth tendency, which is determined by thermodynamics, the crystal growth paths are mainly dependent on the kinetics. Therefore, metal nanoparticles at various transition states that are metastable thermodynamically could be generated by carefully controlling the growth kinetics.

A number of suitable techniques have been developed to satisfactorily tailor the size and size distribution of nanoparticles through balancing the relative

depletion of monomers between the nucleation and growth stages, e.g. hot injection, delayed nucleation, and digestive ripening [5, 422–430]. It is also noteworthy that the capping agents can affect the specific surface energy of the growing nanoparticles, which has important implications in the tuning of their shape [5, 142, 428]. In brief, facet-preferential ligand adhesion can modify the relative growth rates along the various crystallographic directions and/or can favor the selective elimination of unstable surfaces by triggering oriented attachment of particles. In the absence of additional circumstances that can interrupt growth symmetry (e.g. the presence of foreign particle catalysts or the application of external electric or magnetic fields), the capping agents remain mostly responsible for the formation of nanoparticles in a variety of anisotropic shapes, such as cubes, polyhedrons, rods, wires, polypods, and rings [142, 143].

The concepts developed for attaining colloidal single-material nanoparticles could be extended to produce more elaborate composite nanomaterials. The formation of nanocomposites (which are featured with one or multiple inorganic interfaces between chemically and structurally different materials) using solution-based syntheses follows the simple principle of the classical nucleation theory, according to which the activation energy for continuous enlargement of the preexisting particles in a solution (i.e. heterogeneous nucleation/growth) is much lower than the barrier for the generation of novel nuclei (i.e. homogeneous nucleation) [431–433]. This concept has been elegantly demonstrated by Cozzoli and coworkers through comparing with the traditional molecular beam epitaxy (MBE) and chemical vapor deposition (CVD) techniques used for accomplishing the formation of multilayered thin-film heterostructures onto crystallographically oriented substrates [143, 146]. As schematically shown in Figure 1.5, when a secondary material (referred to as "2" in the sketch) has to be deposited over a preexisting seed substrate of a different material (denoted as "1"), the sign of total Gibbs free surface energy change function, ΔG_S, that accompanies the heterogeneous deposition process, will dictate the tendency of the system to adopt a given growth mode [431]:

$$\Delta G_S = \gamma_1 - \gamma_2 + \gamma_{1,2} \tag{1.1}$$

where γ_1 and γ_2 are the surface energies associated with the respective materials (the solid/solution interfacial energies in the case of colloidal nanostructure in a liquid medium) and $\gamma_{1,2}$ is the solid/solid interfacial energy. The former two terms can be expected to be influenced by adhesion of foreign species (e.g. surfactants, ligands, monomers), while the latter depends on the bonding strength and degree of crystallographic compatibility of the concerned lattices.

If the secondary material exposes lower energy surfaces ($\gamma_2 < \gamma_1$) and/or attains good crystallographic matching with the substrate ($\gamma_{1,2}$ is small), then its deposition will likely take place layer by layer, resulting in a continuous and uniform coverage ($\Delta G_S > 0$: *Frank–van der Merwe* mode in Figure 1.5a). As opposed to this, if the secondary material is featured by higher energy surfaces ($\gamma_2 > \gamma_1$) and/or is significantly lattice mismatched ($\gamma_{1,2}$ is high), then it will tend to deposit adopting the habit of a discontinuous island-like domain array as a means of minimizing the overall interfacial area shared with the seed substrate underneath ($\Delta G_S < 0$: *Volmer–Weber* mode in Figure 1.5b). Another possibility

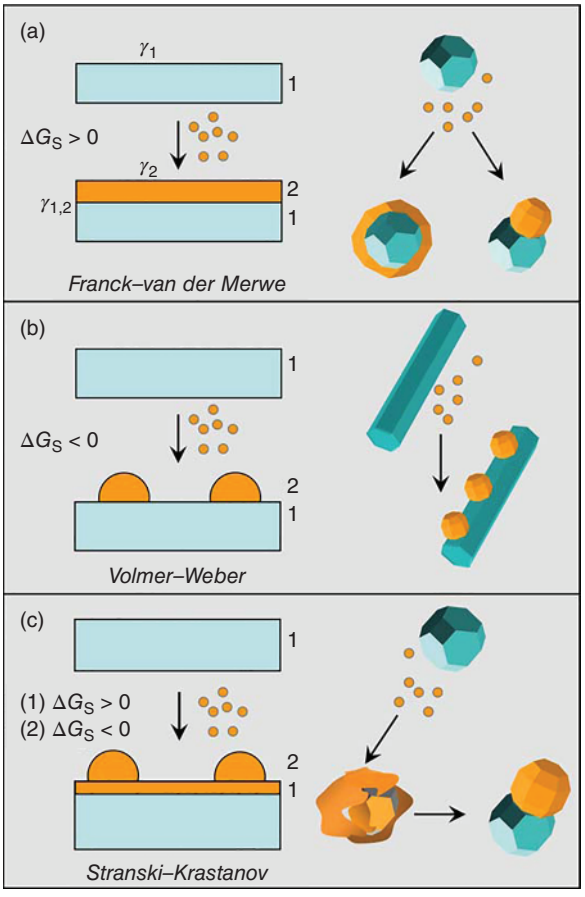

Figure 1.5 Comparative sketches illustrating possible heterogeneous deposition modes for a secondary material (referred to as "2") that is deposited from the respective molecular precursors onto a preformed seed substrate of a different material (referred to as "1"): (a) *Franck–van der Merwe*; (b) *Volmer–Weber*; and (c) *Stranski–Krastanov* regimes. Source: Carbone and Cozzoli 2010 [146]. Adapted with permission of Elsevier.

may involve a progressive two-mode deposition regime (*Stranski–Krastanov* mode in Figure 1.5c). In the early stages, the secondary material forms according to a layer-by-layer growth ($\Delta G_S > 0$). Subsequently, as the deposited layer exceeds a critical thickness, segregation into discrete islands can be observed ($\Delta G_S < 0$) in response to the significant intensification of interfacial strain fields.

According to the scheme in Figure 1.5, the environment for generating nanocomposites contains preformed nanoparticles of a target material, referred to as the "seeds," which serve as primary substrate centers for accommodating secondary inorganic domains of different materials upon reaction of the respective molecular precursors. On the basis of the key principle of the classical nucleation theory [142, 143, 428, 434], the energy barrier, ΔG^*_{het}, that has to be surpassed for a given material to nucleate heterogeneously onto a preexisting condensed phase (the seeds) is lower than the activation energy, ΔG^*_{hom}, required to induce corresponding homogeneous nucleation of separate crystal embryos:

$$\Delta G^*_{het} = f(\theta)\Delta G^*_{hom} \tag{1.2}$$

where the "wetting" function, $0 < f(\theta) < 1$, depends on the particular system geometry (e.g. size/shape of the seed substrates and of the material

domains deposited thereon) and on the tension equilibrium attained at the three-boundary seed/domain/solution region. Note that the barrier for the growth of the heterogeneously nucleated domain, $\Delta G^*_{\text{growth}}$, is far smaller than both ΔG^*_{hom} and ΔG^*_{het} and corresponds to the limiting case of complete wetting ($f(\theta) \rightarrow 0$ for $\theta \rightarrow 0$). In an equivalent way, heterogeneous nucleation can be understood as requiring a much lower chemical potential of solution monomers (proportional to their concentration) to be triggered, relative to homogeneous nucleation:

$$\Delta\mu_{\text{het}} < \Delta\mu_{\text{hom}} \tag{1.3}$$

The deposition regimes predicable on the basis of the evolution of the ΔG_S function sign (Eq. 1.1) can be equally translated to the context of a seed-mediated growth synthesis, whereby the energy gain justifying the preference for a given topological configuration arises from a compensation mechanism by which the surface and interfacial energy terms (Eq. 1.1) conveniently offset with each other. For instance, following heterogeneous deposition on a highly faceted seed, a secondary material can either attain continuous shell (hence, leading to a composite particle with an onion-like geometry) or develop into a discrete section (hence, giving rise to a dimeric heteroproduct), if complete "wetting" is either realized for any of the facets exposed, or selectively for just a few of them, respectively (Figure 1.5a). On the other hand, under conditions favoring only partial "wetting" regime, one or more sufficiently extended facets of the original seeds can accommodate multiple domains of the foreign material (Figure 1.5b). As an intermediate evolutionary case, a transformation from a metastable onion-like architecture (e.g. core–shell particles with an amorphous shell) to a phase-segregated dimeric heterostructure could be expected as a convenient pathway toward lowering of interfacial strain as crystallization proceeds (Figure 1.5c).

At this point, it is noteworthy that the creation of nanoscale heterointerfaces in solution can greatly profit from binding of organic stabilizers or other solution species, which can significantly impact the surface energy terms (i.e. γ_1 and γ_2 terms) and therefore alter the ultimate Gibbs free energy balance. This potentially transcribes into a unique flexibility in the synthesis of nanocomposites made of structurally dissimilar materials arranged in nonequivalent topologies, provided that properly engineered seeds are combined with heterogeneous deposition routes characterized by suitable ΔG^*_{het} and ΔG^*_{hom} parameters. However, the interplay of kinetic processes associated, for example, with solution supersaturation, reactant diffusion, and/or the inherent chemical reactivity of the seeds and/or the particular molecular precursor selected, as well as operation of unusual mechanisms by which misfit strain may be relieved can greatly complicate mechanistic interpretation.

Although these general concepts have made significant successes for preparing noble metal-based nanocomposites with controlled sizes/shapes, gaining a comprehensive understanding of how nanocomposites form is still very challenging. With respect to a large number of wet chemistry methods for synthesizing noble metal-based nanocomposites, in the following chapters of this book,

various growth mechanisms accounting for noble metal-based nanocomposites with different configurations are introduced.

1.4 Characterizations of Composite Nanomaterials

The progress of nanoscience and nanotechnology is largely owing to the rapid development of material characterization techniques, which allow us to directly observe the structure details of the materials at the nanometer scale as well as to measure and manipulate the physical and chemical properties of the nanomaterials. In the case of nanocomposites consisting of noble metals and semiconductors or metal oxides, Fourier transform infrared (FT-IR) and ultraviolet–visible (UV–vis) absorption spectroscopies can be normally employed to characterize their structural functions and ligand integrity [276]. FT-IR spectroscopy can provide the information on functional group identities of the capping agents, while UV–vis spectroscopy can be used to monitor the changes in plasmonic absorption of noble metals, particularly for Au and Ag [170–173, 239].

X-ray diffraction (XRD) is a commonly used tool to determine the composition of nanocomposites through characterizing the crystal phase of different domains in the composite nanomaterials. For the composite particles dispersed in nonpolar organic solvents such as toluene, dichloromethane, and hexane, sample preparation for XRD analysis usually begins with concentrating the colloidal solution to 0.5 ml using flowing Ar or N_2. Methanol or ethanol is then added to precipitate the nanocomposites, which are then recovered by centrifugation and washed with methanol or ethanol several times to remove nonspecifically bound capping agents, e.g. oleylamine, alkylamine, and alkanethiol. The nanocomposites are finally dried at room temperature in vacuum. For the composite particles dispersed in polar solvent, e.g. water, the nanocomposites could be collected by direct centrifugation or firstly transferred into nonpolar organic solvents, followed by recovering using methanol or ethanol precipitation. XRD is usually not solely used to deduce the formation of composite nanostructures as in the case of core–shell-structured nanocomposites with ultrathin shells, the shell phase might not be detected by XRD due to the change in lattice parameters of the shell component.

X-ray photoelectron spectroscopy (XPS) is an electron spectrum based on photoelectric effect. It uses X-ray photons to excite the inner electrons of the surface atoms of the substance, and obtain the energy spectrum by energy analysis of these electrons. In the field of nanoscience and technology, the most common application of XPS is the analysis of surface composition and chemical valence of the nanomaterials. Sample preparation for XPS is analogous to that for XRD. After collection, the composite particles are pasted on a sample holder for XPS measurements. XPS is an extremely important tool to analyze the lattice strain effect (surface strain induced by growing a desired material on other materials with different lattice constants) and electronic coupling effect (electronic interaction induced due to energy level alignments or difference in electronegativity) in noble metal-based nanomaterials with composite or other heterogeneous

structures [141, 316, 398, 405, 435]. Through strong interaction between different domains in these composite nanostructures, the lattice strain effect and electronic coupling effect often induce the shifts in binding energies of the corresponding metal components, which can be sensitively detected by XPS.

In addition, other techniques such as thermogravimetric analysis (TGA) could provide the mass percentage of capping agents in nanocomposites at different decomposition temperatures. The metal contents in the nanocomposites could be accurately determined by inductively coupled plasma atomic emission spectroscopy (ICP-AES).

Although the spectroscopic tools have been extensively used to obtain the fundamental structural and compositional information about the composite nanomaterials, they do not exhibit high spatial resolution. By comparison, microscopy is perhaps the most popular technique adopted to characterize materials at nanometer scales. Transmission electron microscopy (TEM) exhibits high spatial resolution, and is an indispensable tool for the characterization of nanostructured materials. It can offer the most intuitive description of the scale, scale distribution, morphology, and structure of nanomaterials. For preparing samples for TEM measurements, a drop of the colloidal solution is usually dispensed onto a 3-mm carbon-coated copper grid. The excessive solution is then removed by an absorbent paper, and the sample is subsequently dried in air or under vacuum at room temperature.

A typical feature of nanomaterials is their small particle size. Although the use of optical spectroscopy, XRD, and XPS can show some structural features of the nanomaterials, only with the use of TEM is it possible to obtain the visual image of particles at nanoscale ranges. The TEM is unique and indispensable because it provides a true spatial image of the nanomaterials and their surface atoms distribution. Up to now, TEM has evolved into a multifunction instrument, which not only provides atomic resolution of the lattice image but also gives the material structure and chemical information in the 1-nm or even higher spatial resolution, so that directly identifying the chemical composition of a single nanocrystal is possible. TEM can not only give an intuitive description of the morphology of a single particle but also can provide its whole mappings, e.g. inner structure, composition, defects, and lattice features, by combining with energy dispersive X-ray spectroscopy (EDX), selected area electron diffraction, high-resolution and high-angle annular dark-field scanning modes.

The most common application of TEM is an intuitive description of the size, morphology, and size distribution of nanoparticles. The observation of the same nanometer system at different times or stages through TEM can reveal the evolution of the physical properties of nanocrystals [82, 83].

Noble metal-based composite nanomaterials often exhibit strong imaging contrast between metal and semiconductor/oxide domains due to the difference in their electron density, which render the structure of nanocomposites easy to be identified. As a typical example, Figure 1.6 shows the TEM images obtained on a Philips EM 420 microscopy for Fe_3O_4–Pt nanocomposites prepared by epitaxial growth of iron onto Pt seed particles with different sizes followed by Fe oxidation [351], in which the Pt and Fe_3O_4 domains as well as their average sizes could be clearly discerned. Further, the details in each domain

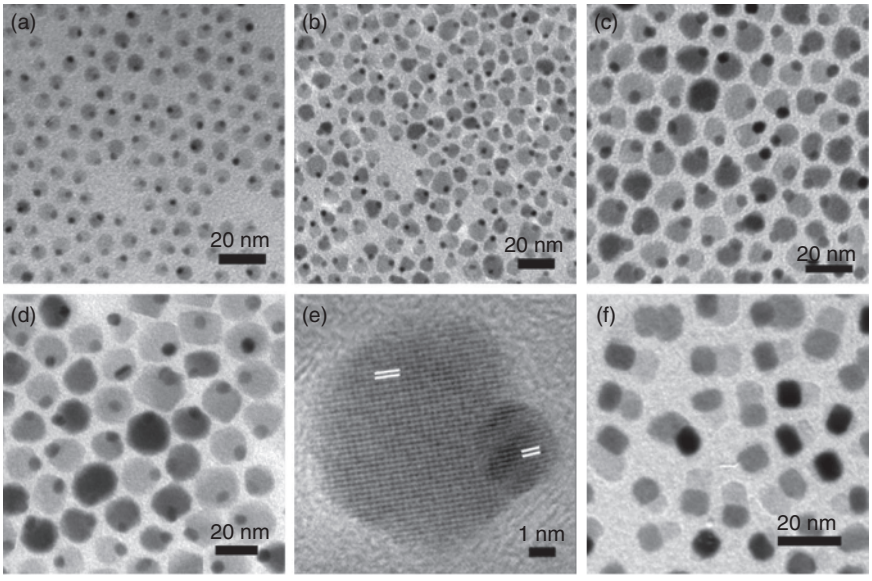

Figure 1.6 TEM images of (a) 3–7 nm, (b) 3–10 nm, (c) 5–12 nm, and (d) 5–17 nm Pt–Fe_3O_4 nanocomposites; (e) HRTEM image of a 3–10 nm Pt–Fe_3O_4 nanocomposites; (f) TEM image of 7–10 nm Pt–Fe_3O_4 nanocomposites with Pt nanocubes as seeds. Source: Wang et al. 2009 [351]. Adapted with permission of American Chemical Society.

of the Fe_3O_4–Pt nanocomposites can be revealed through analyzing the TEM images in high-resolution mode. As indicated in Figure 1.6e, the HRTEM image recorded by a JEOL 2010 microscopy for a 10- to 3-nm Fe_3O_4–Pt composite particle suggests the epitaxial relation between Pt and Fe_3O_4. The distance between two lattice fringes in 10-nm Fe_3O_4 measured from the HRTEM image is 0.22 nm, close to (400) plane spacing (0.212 nm) in inverse spinel structured Fe_3O_4, while the interfringe distance in 3-nm Pt is 0.20 nm, corresponding to (200) plane spacing (0.196 nm) in face-centered cubic (fcc) Pt. The epitaxial relation between Pt and Fe_3O_4 is also confirmed by the controlled growth of Fe on the cubic Pt seeds. Figure 1.6f shows the TEM image of the 10- to 7-nm Fe_3O_4–Pt nanocomposites obtained from the growth of Fe on the 7-nm Pt cubic seeds followed by air oxidation of Fe. It can be seen that the Fe_3O_4 grows on one face of each Pt cube and adopts a cube-like morphology.

For the noble metal-based nanocomposites synthesized via seed-mediated growth, by combing the TEM observation at scanning mode with the EDX analysis, the structural information could be clarified. As a typical example, Figure 1.7 shows the element mappings of two individual intermediates during the formation of heterogeneous trimeric Fe_3O_4–Pt–Ag nanocomposites using dimeric Fe_3O_4–Pt as seeds, in which the corresponding STEM-EDX maps for Ag and an overlay of Ag, Pt, and Fe clearly manifest that several Ag domains attached to both the Pt and Fe_3O_4 surfaces. These observations support the conclusion that the chemoselective addition of Ag to Pt–Fe_3O_4 dimeric seeds

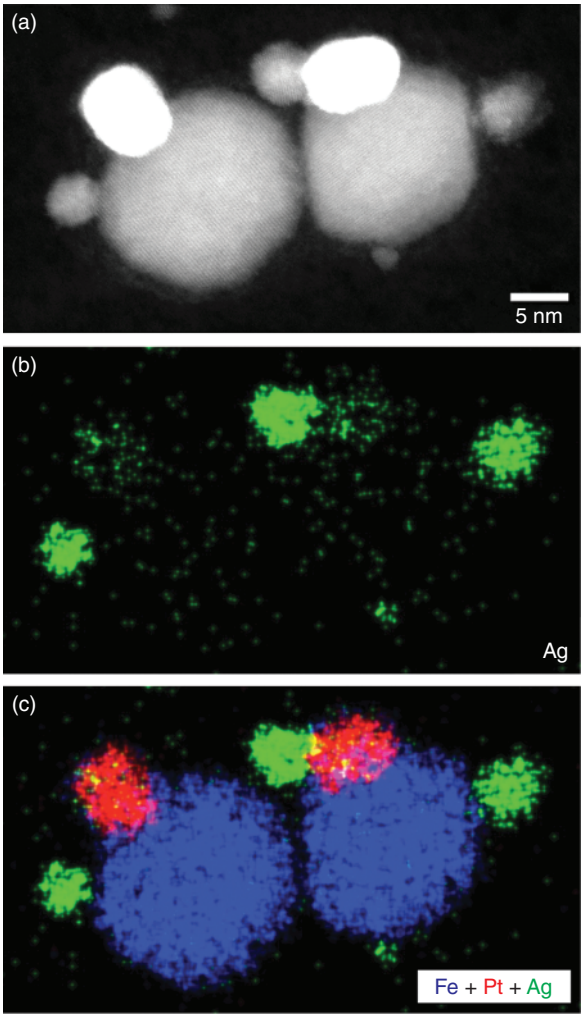

Figure 1.7 (a) High-magnification HAADF-STEM image showing a representative Ag–(Pt–Fe_3O_4) intermediate from the aliquot taken at 60 minutes into the Ag–Pt–Fe_3O_4 reaction. The nanoparticles display small domains attached to the Pt and Fe_3O_4 surfaces of the Pt–Fe_3O_4 seeds, which are confirmed to be Ag in the corresponding EDX elemental maps shown in parts (b) and (c). Source: Hodges et al. 2015 [386]. Adapted with permission of American Chemical Society.

occurs through multiple Ag nucleation events, followed by coalescence onto the Pt domain to form the final Fe_3O_4–Pt–Ag trimeric nanocomposites.

It is noteworthy that characterization of the nanomaterials using TEM requires that the particle image must be obtained with right focus or only a slight deviation from the focus (with respect to the proficiency of the operators). If large deviation from the right focuses (i.e. large underfocus or overfocus) occurs, the image information obtained for the samples will be completely wrong.

1.5 The Scope of This Book

In recent years, there have been tremendous developments in high degree of control over nanocomposites in terms of their domain size, morphology, and

composition. Further, extensive applications emerge in the field of photocatalysis, as nanoscale sections of certain semiconductors or metal oxides combined with appropriate noble metals as cocatalysts could allow the photogenerated charge carriers to separate effectively for performing redox reactions with high efficiency. Therefore, the potential for photocatalytic applications will be expected to scale dramatically with an increase in the complexity of nanocomposites that can be fabricated. In addition, composite nanomaterials based on noble metals would be particularly useful for electrocatalytic applications. Adjacent domains of semiconductors or metal oxides having different electron affinity and appropriate energy-level alignment could either donate or withdraw electrons from the noble metal domain through the permanent inorganic interfaces of the nanocomposites, thus inducing the changes of the electron density around the metal atoms. The changes in electron density would tune the catalytic property of noble metals by altering the adsorption/desorption of reactants on the noble metal catalysts.

We therefore prefer to devote this book to summarize the developments of solution-based methods for the preparation of noble metal-based nanocomposites, their characterization, and potential applications in catalysis so as to provide the readers with a systematic and coherent picture of the field. Most of these works have only been carried out in the past several years. Regarding the creation of great opportunities and tremendous challenges due to the accumulation in nanocomposites, in each chapter and the final section of this book, we put forth some perspectives for the future development of the noble metal-based composite nanomaterials as well as their associated techniques and applications. We hope that through this research effort, one can learn and expect the future progress in synthetic ability would open up access to new breeds of nanomaterials with multiple functionalities, which could enable optical, optoelectronic, magnetic, biomedical, photovoltaic, and specifically catalytic applications with a high level of performance.

Synthesis of nanocomposites consisting of chemical distinct components often requires specific solvent environments, and this makes phase transfer an important technique in the fabrication of various nanostructures. Therefore, following the first chapter, we devote Chapter 2 to introduce an ethanol-mediated phase transfer method, which is generic enough to transfer both metal ions and nanoparticles from aqueous solution to a nonpolar organic medium. The transfer protocol involves mixing the aqueous solution of metal ions or nanoparticles with an ethanolic solution of dodecylamine (DDA), and extracting the coordinating compounds formed between metal ions/nanoparticles and DDA into toluene. This ethanol-mediated protocol could be applied toward transferring a wide variety of transition and noble metal ions with efficiencies higher than 95%, and allows the synthesis of a large variety of metallic and semiconductor nanocrystals to be performed in organic media using relatively inexpensive water-soluble metal salts as starting precursors, thus offering necessary solvent surroundings for the wet chemistry-based synthesis of nanomaterials. It is therefore an important step preceding the fabrication of noble metal-based nanocomposites with multiple functionalities.

In Chapter 3, we start with a universal phosphine-free synthesis for metal selenide nanocrystals, which might serve as seeds for the further fabrication of semiconductor–noble metal nanocomposites. In this method, reduction of elemental selenide (Se) with sodium borohydride in the presence of hydrophobic alkylamines generates hydrophobic alkylammonium selenide species *in situ*. The phosphine-free Se precursor is highly reactive, and suitable for the synthesis of various metal selenide nanocrystals. Its high reactivity is also favorable to derive core–shell CdSe@CdS quantum dots (QDs) in one-pot synthesis, without the need for prior purification of CdSe cores, offering a greener and less expensive route to the large-scale synthesis of metal selenide QDs. In the latter sections of the chapter, we conduct a careful review on the advances in the literatures associated with nanocomposites consisting of chalcogenide semiconductors and gold, the topics being studied most sufficiently. Afterwards, the chapter focuses on the experimental observations and mechanistic analyses on the composite nanosystems consisting of metal sulfide and Au or/and Ag noble metals derived from the ethanol-mediated transfer of metal ions. In the final section of the chapter, the applications of a number of semiconductor–gold nanocomposites in the synthesis of propargylic amines via a three-component coupling reaction of aldehyde, amine, and alkyne in water are demonstrated.

Chapter 4 reviews the nanocomposites consisting of chalcogenide semiconductors and noble metals other than gold, mainly including Ag and Pt, as well as their application in photocatalytic hydrogen generation. Motivated by their unique property and great potential particularly in photocatalysis, nanocomposites consisting of semiconductor and noble metals other than gold have also received significant attention in recent years. These types of fascinating nanocomposites based on radically different approaches are presently being developed and many others remain to be exploited. In this respect, this and the following chapters may provide different examples of some new uncharted territories opened in different lines of the general field of composite nanomaterials.

Chapter 5 aims at presenting a facile, aqueous route for the synthesis of nanocomposites consisting of silver sulfide (Ag_2S) and different noble metals. By reducing various noble metal precursors using citrate in aqueous phase in the presence of preformed Ag_2S nanocrystals, uniform semiconductor–noble metal heterogeneous nanostructures are obtained as the dominant product. In addition to binary nanocomposites, ternary and quaternary hybrid systems are also achieved via the successive deposition of different noble metals on the surface of Ag_2S nanocrystals. A number of characterization techniques, including TEM, HRTEM, high-angle annular dark-field scanning TEM (HAADF-STEM), XRD, EDX, and XPS are employed to characterize the morphology of the finally formed nanocomposites. In particular, the Pt-containing nanocomposites are found to exhibit superior catalytic activity toward methanol oxidation reaction (MOR), the key reaction in direct methanol fuel cells (DMFCs), due to the electronic coupling effect between the ultrafine Pt crystallites and the semiconductor domains.

Chapter 6 demonstrates the general synthesis of nanocomposites consisting of silver chalcogenides (Ag_2S or Ag_2Se) and noble metal nanoparticles with a hollow or cage-bell structure for effectively coupling the various effects specific to

the different domains of the nanocomposite for greater application versatility. The synthesis is based on the inside-out diffusion of silver (Ag) in core–shell nanoparticles. It begins with the preparation of core–shell nanoparticles, in which Ag is located at the core or inner shell region. The Ag is then removed from the core or from the internal shell and converted into Ag_2S or Ag_2Se by chalcogenide precursors, e.g. elemental sulfur, sodium sulfide, or sodium selenide. The Ag_2S or Ag_2Se forms the semiconductor domain in the nanocomposite and shares solid-state interfaces with the remaining hollow or cage-bell-structured metal nanoparticles. The structural transformation from core–shell to heterogeneous nanocomposites may provide new opportunities to design and fabricate hybrid nanostructures with interesting physicochemical properties.

Engineering the structure of Pt nanoparticles is an effective approach to improve their catalytic activity on a mass basis. Chapter 7 demonstrates a strategy for the synthesis of CdSe–Pt nanocomposites with a core–shell construction and evaluates their catalytic properties in room temperature ORR and MOR. By reducing Pt precursors with sodium citrate in the presence of previously formed CdSe nanocrystals in aqueous phase, uniform core–shell CdSe@Pt nanocomposites are obtained as the dominant product. The inner-placed CdSe core is not only helpful for saving substantial amount of valuable platinum metals but also offers a vivid example to investigate the lateral strain effect exerted by the substrate on the deposited layers, and its influence on the catalytic activity of metal catalysts.

Chapter 8 demonstrates the exploration of Pt-containing semiconductor–noble metal nanocomposites as selective electrocatalysts for DMFCs. Pt-based nanocomposites with enhanced catalytic activity and high selectivity for DMFC reactions are designed and fabricated for sufficiently making use of the structural uniqueness and electronic coupling effects among the different domains of the composite electrocatalysts so that the DMFCs can be operated well without or with little dependence on the proton exchange membrane. This chapter emphasizes the controllable syntheses, characterizations, and electrochemical measurements of the Pt-based nanocomposites and the evaluation of their performance as selective catalysts in a prototype of membraneless DMFC and a DMFC operated using high-concentration methanol as fuel. The intrinsic relationship between the catalytic properties and the synergistic effects in the Pt-based nanocomposites might provide for theoretical and technical bases for effectively developing electrocatalysts with low cost, enhanced activity, and high selectivity.

Chapter 9 introduces the research advances in the synthesis and application of nanocomposites consisting metal oxides and noble metals, particularly highlights the general strategies to produce dumbbell-like nanocomposites that contain noble metal and magnetic nanoparticles, and illustrates the interesting optical and magnetic properties found in these composite particles. Then the chapter focuses on the innovative strategies developed in recent years for underpinning oxide-based nanocomposites with atomic dispersion of noble metals as electrode materials for supercapacitors and as highly efficient catalysts for oxidation of volatile organic compounds (VOCs). The procedures and the information provided in the chapter are general and beneficial, and may suggest

a competent way to efficiently utilize the noble metals and offer a constructive concept to design cost-effective and more active noble metal-based composite materials for energy storage and environmental remediation.

In Chapter 10, we aim at introducing a number of interesting scientific phenomena observed during the syntheses and characterizations of composite nanomaterials. The mechanisms behind these scientific issues and their potential applications are also discussed in the chapter based on the specific features of these discoveries. These interesting scientific phenomena or physical/chemical processes would not only satisfy everlasting human curiosity but also promise new advances in nanoscience and nanotechnology, e.g. design of complicated noble metal-based nanocomposites and highly efficient electrocatalysts with superior activity and durability.

1.6 The Road Ahead

As we review in this work, the overall size of noble metal-based heterogeneous nanocomposites produced using current solution-based approaches is no smaller than 10 nm, and this is not optimum for catalysis. Next, reducing the overall size of the composite nanomaterials might be an effective way to obtain highly efficient catalysts. In this sense, using Au or Ag nanoclusters with average size of c. 1 nm as starting materials to prepare nanocomposites consisting of noble metals and semiconductors/metal oxides might be considered. The finer overall sizes of composite nanomaterials may further boost their activity, durability and selectivity for diverse catalytic reactions.

The synthetic strategies already demonstrated and currently available provide a wide range of composite nanomaterials with various physical/chemical characters. The high degree of control over their sizes, compositions, and morphologies is of particular interest, with achievement of site-, facet-, and shape-specific selective metal deposition. The progress in this field, which is expected to further continue and intensify in the coming years, is directed toward achieving nanocomposites with increased changes in their metal and semiconductor parts, e.g. increased compositions and sophisticated architectures for further tailoring the catalytic, synergistic optical, electronic, and electrical properties of the semiconductor–metal interfaces.

Recent research efforts have demonstrated the great potentials of Pt- or Pd-containing semiconductor–noble metal nanocomposites in electrocatalysis due to the electron coupling effect among their different domains. By optimizing both the composition and domain sizes for the composite nanosystems, further enhancement in their electrocatalytic property could be expected. The semiconductor–metal nanocomposites could also be of interest as advanced functional materials, and as catalysts for other reactions, such as organic and pharmaceuticals synthesis, environmental catalysis, and oxidation/combustion reactions. Further challenges in noble metal-based composite nanomaterials are to enlarge the selection of noble metals and semiconductors via known and innovative synthetic strategies for developing nanocomposites with more

combinations, architectures, and higher complexity so than the coupling effect among different domains or components could be maximized and optimized. This would render the composite nanomaterials more favorable for given technological applications.

Combining conventional wet chemistry methods for synthesizing metal oxide–noble metal nanocomposites with the galvanic replacement reaction offers an effective approach to control the deposition and dispersion of different noble metals on the surface of metal oxide substrates. The procedures may provide for a competent way to efficiently utilize the noble metals and offer a constructive concept to design cost-effective and more active noble metal-based composite materials for energy storage and environmental remediation.

Regarding the creation of great opportunities and tremendous challenges due to the accumulation in nanocomposites, in the final chapter of this book (Chapter 11), we put forth some perspectives for the future development of the metal-based composite nanomaterials. The human being is interfacing a number of forefront research areas in this period of technology development. Through the research efforts on using wet chemistry methods to integrate materials with distinct physical and chemical properties into a single nanosystem for providing multiple functionalities, the scientific communities wish to establish innovative methodologies to influence a rethinking of the current processing technologies: to move toward molecular-level control and regulation; and away from the "top-down" approach and the stringent and expensive control inherent in conventional manufacturing processes.

References

1 Narayanan, R. and El-Sayed, M.A. (2003). *J. Phys. Chem. B* 107: 12416–12424.
2 Narayanan, R. and El-Sayed, M.A. (2004). *Nano Lett.* 4: 1343–1348.
3 Narayanan, R. and El-Sayed, M.A. (2004). *J. Am. Chem. Soc.* 126: 7194–7195.
4 Daniel, M.C. and Astruc, D. (2004). *Chem. Rev.* 104: 293–346.
5 Burda, C., Chen, X., Narayanan, R., and El-Sayed, M.A. (2005). *Chem. Rev.* 105: 1025–1102.
6 Wang, C., Daimon, H., Lee, Y. et al. (2007). *J. Am. Chem. Soc.* 129: 6974–6975.
7 Tian, N., Zhou, Z.Y., Sun, S. et al. (2007). *Science* 316: 732–735.
8 Wang, C., Daimon, H., Onodera, T. et al. (2008). *Angew. Chem. Int. Ed.* 47: 3588–3591.
9 Antolini, E., Lopes, T., and Gonzalez, E.R. (2008). *J. Alloys Compd.* 461: 253–262.
10 Zhang, Q., Xie, J., Yang, J., and Lee, J.Y. (2009). *ACS Nano* 3: 139–148.
11 Tsung, C.K., Kuhn, J.N., Huang, W. et al. (2009). *J. Am. Chem. Soc.* 131: 5816–5822.
12 Chen, J., Lim, B., Lee, E.P., and Xia, Y. (2009). *Nano Today* 4: 81–95.
13 Peng, Z. and Yang, H. (2009). *Nano Today* 4: 143–164.

14 Xia, Y., Xiong, Y., Lim, B., and Skrabalak, S.E. (2009). *Angew. Chem. Int. Ed.* 48: 60–103.
15 Talapin, D.V., Lee, J.-S., Kovalenko, M.V., and Shevchenko, E.V. (2010). *Chem. Rev.* 110: 389–458.
16 Chen, A. and Holt-Hindle, P. (2010). *Chem. Rev.* 110: 3767–3804.
17 An, K. and Somorjai, G.A. (2012). *ChemCatChem* 4: 1512–1524.
18 Calle-Vallejo, F., Martínez, J.I., García-Lastra, J.M. et al. (2014). *Angew. Chem. Int. Ed.* 53: 8316–8319.
19 Cao, S., Tao, F.F., Tang, Y. et al. (2016). *Chem. Soc. Rev.* 45: 4747–4765.
20 Xiong, Y. and Xia, Y. (2007). *Adv. Mater.* 19: 3385–3391.
21 Grzelczak, M., Pérez-Juste, J., Mulvaney, P., and Liz-Marzán, L.M. (2008). *Chem. Soc. Rev.* 37: 1783–1791.
22 Rycenga, M., Cobley, C.M., Zeng, J. et al. (2011). *Chem. Rev.* 111: 3669–3712.
23 Chen, H., Shao, L., Li, Q., and Wang, J. (2013). *Chem. Soc. Rev.* 42: 2679–2724.
24 Gao, M.-R., Xu, Y.-F., Jiang, J., and Yu, S.-H. (2013). *Chem. Soc. Rev.* 42: 2986–3017.
25 Shen, S. and Wang, Q. (2013). *Chem. Mater.* 25: 1166–1178.
26 Fenger, R., Fertitta, E., Kirmse, H. et al. (2012). *Phys. Chem. Chem. Phys.* 14: 9343–9349.
27 Narayanan, R. and El-Sayed, M.A. (2005). *J. Phys. Chem. B* 109: 12663–12676.
28 Zhang, H., Jin, M., Xiong, Y. et al. (2013). *Acc. Chem. Res.* 46: 1783–1794.
29 Brown, K.R., Walter, D.G., and Natan, M.J. (2000). *Chem. Mater.* 12: 306–313.
30 Xiong, Y., Chen, J., Wiley, B. et al. (2005). *J. Am. Chem. Soc.* 127: 7332–7333.
31 Xiong, Y., Chen, J., Wiley, B., and Xia, Y. (2005). *Nano Lett.* 5: 1237–1242.
32 Xiong, Y., Cai, H., Wiley, B.J. et al. (2007). *J. Am. Chem. Soc.* 129: 3665–3675.
33 Lim, B., Xiong, Y., and Xia, Y. (2007). *Angew. Chem. Int. Ed.* 46: 9279–9282.
34 Viswanath, B., Kundu, P., Halder, A., and Ravishankar, N. (2009). *J. Phys. Chem. C* 113: 16866–16883.
35 Chen, D.H., Yeh, J.J., and Huang, T.C. (1999). *J. Colloid Interface Sci.* 215: 159–166.
36 Devarajan, S., Bera, P., and Sampath, S. (2005). *J. Colloid Interface Sci.* 290: 117–129.
37 Xiong, Y., McLellan, J.M., Chen, J. et al. (2005). *J. Am. Chem. Soc.* 127: 17118–17127.
38 Xiong, Y., Washio, I., Chen, J. et al. (2006). *Langmuir* 22: 8563–8570.
39 Wiley, B.J., Xiong, Y., Li, Z.-Y. et al. (2006). *Nano Lett.* 6: 765–768.
40 Washio, I., Xiong, Y., Yin, Y., and Xia, Y. (2006). *Adv. Mater.* 18: 1745–1749.
41 Wiley, B.J., Wang, Z., Wei, J. et al. (2006). *Nano Lett.* 6: 2273–2278.

42 Xiong, Y., Cai, H., Yin, Y., and Xia, Y. (2007). *Chem. Phys. Lett.* 440: 273–278.
43 Chen, D., Yao, Q., Cui, P. et al. (2018). *ACS Appl. Energy Mater.* 1: 883–890.
44 Habas, S.E., Lee, H., Radmilovic, V. et al. (2007). *Nat. Mater.* 6: 692–697.
45 Chen, Y.-H., Huang, H., and Huang, M.H. (2009). *J. Am. Chem. Soc.* 131: 9114–9121.
46 Yu, Y., Zhang, Q., Lu, X., and Lee, J.Y. (2010). *J. Phys. Chem. C* 114: 11119–11126.
47 Wang, A., Peng, Q., and Li, Y. (2011). *Chem. Mater.* 23: 3217–3222.
48 Wang, C., Ye, F., Liu, C. et al. (2011). *Colloids Surf., A* 385: 85–90.
49 Ye, F., Liu, H., Yang, J.H. et al. (2013). *Dalton Trans.* 42: 12309–12316.
50 Chen, D., Li, J., Cui, P. et al. (2016). *J. Mater. Chem. A* 4: 3813–3821.
51 Yang, J., Lee, J.Y., Too, H.-P., and Valiyaveettil, S. (2006). *J. Phys. Chem. B* 110: 125–129.
52 Peng, Z., Wu, J., and Yang, H. (2009). *Chem. Mater.* 22: 1098–1106.
53 Liu, H., Qu, J., Chen, Y. et al. (2012). *J. Am. Chem. Soc.* 134: 11602–11610.
54 Chen, D., Cui, P., He, H. et al. (2014). *J. Power Sources* 272: 152–159.
55 Liu, H. and Yang, J. (2014). *J. Mater. Chem. A* 2: 7075–7081.
56 Liu, H., Ye, F., and Yang, J. (2014). *Ind. Eng. Chem. Res.* 53: 5925–5931.
57 Hou, P., Cui, P., Liu, H. et al. (2015). *Nano Res.* 8: 512–522.
58 Peng, Z.A. and Peng, X. (2001). *J. Am. Chem. Soc.* 123: 1389–1395.
59 Pileni, M.-P. (2003). *Nat. Mater.* 2: 145–150.
60 Lee, S.-M., Cho, S.-N., and Cheon, J. (2003). *Adv. Mater.* 15: 441–444.
61 Yin, Y. and Alivisatos, A.P. (2004). *Nature* 437: 664–670.
62 Lisiecki, I. (2005). *J. Phys. Chem. B* 109: 12231–12244.
63 de Mello Donegá, C., Liljeroth, P., and Vanmaekelbergh, D. (2005). *Small* 1: 1152–1162.
64 Kumar, S. and Nann, T. (2006). *Small* 2: 316–329.
65 Caswell, K.K., Bender, C.M., and Murphy, C.J. (2003). *Nano Lett.* 3: 667–669.
66 Lifshitz, E., Bashouti, M., Kloper, V. et al. (2003). *Nano Lett.* 3: 857–862.
67 Tang, K.-B., Qian, Y.-T., Zeng, J.-H., and Yang, X.-G. (2003). *Adv. Mater.* 15: 448–450.
68 Yu, H. and Buhro, W.E. (2003). *Adv. Mater.* 15: 416–419.
69 Yu, H., Li, J., Loomis, R.A. et al. (2003). *J. Am. Chem. Soc.* 125: 16168–16169.
70 Grebinski, J.W., Hull, K.L., Zhang, J. et al. (2004). *Chem. Mater.* 16: 5260–5272.
71 Chang, S.-S., Lee, C.-L., and Wang, C.R.C. (1997). *J. Phys. Chem. B* 101: 6661–6664.
72 Manna, L., Scher, E.C., and Alivisatos, A.P. (2000). *J. Am. Chem. Soc.* 122: 12700–12706.
73 Cordente, N., Respaud, M., Senocq, F. et al. (2001). *Nano Lett.* 1: 565–568.
74 Kim, F., Song, J.H., and Yang, P. (2002). *J. Am. Chem. Soc.* 124: 14316–14317.

75 Ahrenkiel, S.P., Mićić, O.I., Miedaner, A. et al. (2003). *Nano Lett.* 3: 833–837.
76 Dumestre, F., Chaudret, B., Amiens, C. et al. (2003). *Angew. Chem. Int. Ed.* 42: 5213–5216.
77 Murphy, C.J., Sau, T.K., Gole, A.M. et al. (2005). *J. Phys. Chem. B* 109: 13857–13870.
78 Sun, Y. and Xia, Y. (2002). *Science* 298: 2176–2179.
79 Gou, L. and Murphy, C.J. (2003). *Nano Lett.* 3: 231–234.
80 Lee, S.-M., Jun, Y.-W., Cho, S.-N., and Cheon, J. (2002). *J. Am. Chem. Soc.* 124: 11244–11245.
81 Zhao, N. and Qi, L. (2006). *Adv. Mater.* 18: 359–362.
82 Liu, H., Ye, F., Yao, Q. et al. (2014). *Sci. Rep.* 4: 3969.
83 Feng, Y., Liu, H., and Yang, J. (2014). *J. Mater. Chem. A* 2: 6130–6137.
84 Puntes, V.F., Zanchet, D., Erdonmez, C.K., and Alivisatos, A.P. (2002). *J. Am. Chem. Soc.* 124: 12874–12880.
85 Chen, S., Fan, Z., and Carroll, D.L. (2002). *J. Phys. Chem. B* 106: 10777–10781.
86 Zhang, P. and Gao, L. (2003). *J. Mater. Chem.* 13: 2007–2010.
87 Zhong, X., Feng, Y., Lieberwirth, I., and Knoll, W. (2006). *Chem. Mater.* 18: 2468–2471.
88 Teng, X., Liang, X., Maksimuk, S., and Yang, H. (2006). *Small* 2: 249–253.
89 Wang, L., Hu, C., Nemoto, Y. et al. (2010). *Cryst. Growth Des.* 10: 3454–3460.
90 Yamauchi, Y., Tonegawa, A., Komatsu, M. et al. (2012). *J. Am. Chem. Soc.* 134: 5100–5109.
91 Zhou, S., Mcllwrath, K., Jackson, G., and Eichhorn, B. (2006). *J. Am. Chem. Soc.* 128: 1780–1781.
92 Peng, Z. and Yang, H. (2009). *Nano Res.* 2: 406–415.
93 Wang, L. and Yamauchi, Y. (2010). *J. Am. Chem. Soc.* 132: 13636–13638.
94 Feng, Y., Ma, X., Han, L. et al. (2014). *Nanoscale* 6: 6173–6179.
95 Jin, R., Cao, Y., Mirkin, C.A. et al. (2001). *Science* 294: 1901–1903.
96 Shankar, S.S., Rai, A., Ankamwar, B. et al. (2004). *Nat. Mater.* 3: 482–488.
97 Liz-Marzán, L.M., Giersig, M., and Mulvaney, P. (1996). *Langmuir* 12: 4329–4335.
98 Toshima, N. and Yonezawa, T. (1998). *New J. Chem.* 22: 1179–1201.
99 Davies, R., Schurr, G.A., Meenan, P. et al. (1998). *Adv. Mater.* 10: 1264–1270.
100 Kim, S.W., Kim, M., Lee, W.Y., and Hyeon, T. (2002). *J. Am. Chem. Soc.* 124: 7642–7643.
101 Taton, T.A., Mirkin, C.A., and Letsinger, R.L. (2000). *Science* 289: 1757–1760.
102 Krasteva, N., Besnard, I., Guse, B. et al. (2002). *Nano Lett.* 2: 551–555.
103 Rai, C.R., OKajima, T., and Ohsaka, T. (2003). *J. Electroanal. Chem.* 543: 127–133.
104 Jaiswal, J.K., Mattoussi, H., Mauro, J.M., and Simon, S.M. (2003). *Nat. Biotechnol.* 21: 47–51.

105 Sukhanova, A., Devy, J., Venteo, L. et al. (2004). *Anal. Biochem.* 324: 60–67.
106 Murphy, C.J. and Jana, N.R. (2002). *Adv. Mater.* 14: 80–82.
107 Rodríguez-González, B., Burrows, A., Watanabe, M. et al. (2005). *J. Mater. Chem.* 15: 1755–1759.
108 Hines, M.A. and Guyot-Sionnest, P. (1996). *J. Phys. Chem.* 100: 468–471.
109 Dabbous, B.O., Rodriguez-Viejo, J., Mikulec, F.V. et al. (1997). *J. Phys. Chem. B* 101: 9463–9475.
110 Peng, X., Schlamp, M.C., Kadavanich, A.V., and Alivisatos, A.P. (1997). *J. Am. Chem. Soc.* 119: 7019–7029.
111 Cao, Y.W. and Banin, U. (2000). *J. Am. Chem. Soc.* 122: 9692–9702.
112 Sashchiuk, A., Langof, L., Chaim, R., and Lifshitz, E. (2002). *J. Cryst. Growth* 240: 431–438.
113 Zeng, H., Li, J., Wang, Z.L. et al. (2004). *Nano Lett.* 4: 187–190.
114 Wang, L., Luo, J., Fan, Q. et al. (2005). *J. Phys. Chem. B* 109: 21593–21601.
115 Jin, R. and Mirkin, C.A. (2001). *J. Am. Chem. Soc.* 123: 7961–7962.
116 Henglein, A. and Giersig, M. (1994). *J. Phys. Chem.* 98: 6931–6935.
117 Kolb, U., Quaiser, S.A., Winter, M., and Reetz, M.T. (1996). *Chem. Mater.* 8: 1889–1894.
118 Luo, J., Wang, L., Mott, D. et al. (2008). *Adv. Mater.* 20: 4342–4347.
119 Tao, F., Grass, M.E., Zhang, Y. et al. (2008). *Science* 322: 932–934.
120 Joo, S.H., Park, J.Y., Tsung, C.-K. et al. (2009). *Nat. Mater.* 8: 126–131.
121 Zhou, W., Yang, X., Vukmirović, M.B. et al. (2009). *J. Am. Chem. Soc.* 131: 12755–12762.
122 Reetz, M.T., Helbig, W., and Quaiser, S.A. (1995). *Chem. Mater.* 7: 2227–2228.
123 Goia, D.V. and Matijević, E. (1998). *New J. Chem.* 22: 1203–1215.
124 Treguer, M., de Cointet, C., Remita, H. et al. (1998). *J. Phys. Chem. B* 102: 4310–4321.
125 Belloni, J., Mostafavi, M., Remita, H. et al. (1998). *New J. Chem.* 22: 1239–1255.
126 Sun, S., Murray, C.B., Weller, D. et al. (1989-1992). *Science* 2000, 287.
127 Rao, C.N.R., Kulkarni, G.U., Thomas, P.J., and Edwards, P.P. (2000). *Chem. Soc. Rev.* 29: 27–35.
128 Shevchenko, E.V., Talapin, D.V., Rogach, A.L. et al. (2002). *J. Am. Chem. Soc.* 124: 11480–11485.
129 Doudna, C.M., Bertino, M.F., and Tokuhiro, A.T. (2002). *Langmuir* 18: 2434–2435.
130 Doudna, C.M., Bertino, M.F., Blum, F.D. et al. (2003). *J. Phys. Chem. B* 107: 2966–2970.
131 Zhou, S., Varughese, B., Eichhorn, B. et al. (2005). *Angew. Chem. Int. Ed.* 44: 4539–4543.
132 Liu, Z., Hu, J.E., Wang, Q. et al. (2009). *J. Am. Chem. Soc.* 131: 6924–6925.
133 Ji, X., Lee, K.T., Holden, R. et al. (2010). *Nat. Chem.* 2: 286–293.
134 Kim, J., Lee, Y., and Sun, S. (2010). *J. Am. Chem. Soc.* 132: 4996–4997.
135 Loukrakpam, R., Luo, J., He, T. et al. (2011). *J. Phys. Chem. C* 115: 1682–1694.

136 Zhang, J., Sasaki, K., Sutter, E., and Adžič, R.R. (2007). *Science* 315: 220–222.
137 Guo, S., Dong, S., and Wang, E. (2008). *J. Phys. Chem. C* 112: 2389–2393.
138 Peng, Z. and Yang, H. (2009). *J. Am. Chem. Soc.* 131: 7542–7543.
139 Lim, B., Jiang, M., Camargo, P.H.C. et al. (2009). *Science* 324: 1302–1305.
140 Kim, Y., Hong, J.W., Lee, Y.W. et al. (2010). *Angew. Chem. Int. Ed.* 122: 10395–10399.
141 Ye, F., Liu, H., Hu, W. et al. (2012). *Dalton Trans.* 41: 2898–2903.
142 Cozzoli, P.D., Pellegrino, T., and Manna, L. (2006). *Chem. Soc. Rev.* 35: 1195–1208.
143 Casavola, M., Buonsanti, R., Caputo, G., and Cozzoli, P.D. (2008). *Eur. J. Inorg. Chem.* 837–854.
144 Yang, J., Sargent, E.H., Kelley, S.O., and Ying, J.Y. (2009). *Nat. Mater.* 8: 683–689.
145 Choi, C.L. and Alivisatos, A.P. (2010). *Annu. Rev. Phys. Chem.* 61: 369–389.
146 Carbone, L. and Cozzoli, P.D. (2010). *Nano Today* 5: 449–493.
147 Costi, R., Saunders, A.E., and Banin, U. (2010). *Angew. Chem. Int. Ed.* 49: 4878–4897.
148 Lattuada, M. and Hatton, T.A. (2011). *Nano Today* 6: 286–308.
149 Yang, J., Lee, J.Y., and Ying, J.Y. (2011). *Chem. Soc. Rev.* 40: 1672–1696.
150 Vaneski, A., Susha, A.S., Rodríguez-Fernández, J. et al. (2011). *Adv. Funct. Mater.* 21: 1547–1556.
151 Buck, M.R. and Schaak, R.E. (2013). *Angew. Chem. Int. Ed.* 52: 6154–6178.
152 Sitt, A., Hadar, I., and Banin, U. (2013). *Nano Today* 8: 494–513.
153 Rawalekar, S. and Mokari, T. (2013). *Adv. Energy Mater.* 3: 12–27.
154 Jiang, R., Li, B., Fang, C., and Wang, J. (2014). *Adv. Mater.* 26: 5274–5309.
155 Nag, A., Kundu, J., and Hazarika, A. (2014). *CrystEngComm* 16: 9391–9407.
156 Banin, U., Ben-Shahar, Y., and Vinokurov, K. (2014). *Chem. Mater.* 26: 97–110.
157 Dutta, S.K., Mehetor, S.K., and Pradhan, N. (2015). *J. Phys. Chem. Lett.* 6: 936–944.
158 Pescaglini, A. and Lacopino, D. (2015). *J. Mater. Chem. C* 3: 11785–11800.
159 Liu, H., Feng, Y., Chen, D. et al. (2015). *J. Mater. Chem. A* 3: 3182–3223.
160 Ben-Shahar, Y. and Banin, U. (2016). *Top. Curr. Chem.* 374: 54.
161 Qu, J., Ye, F., Chen, D. et al. (2016). *Adv. Colloid Interface Sci.* 230: 29–53.
162 Biteen, J.S., Pacifici, D., Lewis, N.S., and Atwater, H.A. (2005). *Nano Lett.* 5: 1768–1773.
163 Liu, M. and Guyot-Sionnest, P. (2006). *J. Mater. Chem.* 16: 3942–3945.
164 Jin, Y. and Gao, X. (2009). *Nat. Nanotechnol.* 4: 571–576.
165 Zhang, J., Tang, Y., Lee, K., and Ouyang, M. (2010). *Nature* 466: 91–95.
166 Achermann, M. (2010). *J. Phys. Chem. Lett.* 1: 2837–2843.
167 Khon, E., mereshchenko, A., Tarnovsky, A.N. et al. (2011). *Nano Lett.* 11: 1792–1799.
168 Shaviv, E., Schubert, O., Alves-Santos, M. et al. (2011). *ACS Nano* 5: 4712–4719.
169 Zeng, J., Tao, J., Su, D. et al. (2011). *Nano Lett.* 11: 3010–3015.
170 Khanal, B.P., Pandey, A., Li, L. et al. (2012). *ACS Nano* 6: 3832–3840.

171 Fang, C., Lee, Y.H., Shao, L. et al. (2013). *ACS Nano* 7: 9354–9365.
172 Jing, H., Large, N., Zhang, Q., and Wang, H. (2014). *J. Phys. Chem. C* 118: 19948–19963.
173 Gordon, T.R. and Schaak, R.E. (2014). *Chem. Mater.* 26: 5900–5904.
174 Muhammed, M.A.H., Döblinger, M., and Rodríguez-Fernández, J. (2015). *J. Am. Chem. Soc.* 137: 11666–11677.
175 Sugimoto, H., Fujii, M., and Imakita, K. (2016). *Nanoscale* 8: 10956–10962.
176 Shahjamali, M.M., Zhou, Y., Zaraee, N. et al. (2016). *ACS Nano* 10: 5362–5373.
177 Jakob, M., Levanon, H., and Kamat, P.V. (2003). *Nano Lett.* 3: 353–358.
178 Subramanian, V., Wolf, E., and Kamat, P.V. (2004). *J. Am. Chem. Soc.* 126: 4943–4950.
179 Salant, A., Amitay-Sadovsky, E., and Banin, U. (2006). *J. Am. Chem. Soc.* 128: 10006–10007.
180 Ni, M., Leung, M.K.H., Leung, D.Y.C., and Sumathy, K. (2007). *Renew. Sustain. Energy Rev.* 11: 401–425.
181 Costi, R., Saunders, A.E., Elmalem, E. et al. (2008). *Nano Lett.* 8: 637–641.
182 Murdoch, M., Waterhouse, G.I.N., Nadeem, M.A. et al. (2011). *Nat. Chem.* 3: 489–492.
183 Seh, Z.W., Liu, S., Low, M. et al. (2012). *Adv. Mater.* 24: 2310–2314.
184 Wang, L., Ge, J., Wang, A. et al. (2014). *Angew. Chem. Int. Ed.* 53: 5107–5111.
185 Jiang, W., Bai, S., Wang, L. et al. (2016). *Small* 12: 1640–1648.
186 Wang, X., Long, R., Liu, D. et al. (2016). *Nano Energy* 24: 87–93.
187 Xu, K., Wu, J., Tian, C.F. et al. (2017). *Nanoscale* 9: 11574–11583.
188 Ma, G., He, J., Rajiv, K. et al. (2004). *Appl. Phys. Lett.* 84: 4684–4686.
189 Lin, H., Chen, Y., Wang, J. et al. (2006). *Appl. Phys. Lett.* 88: 161911.
190 Mongin, D., Shaviv, E., Maioli, P. et al. (2012). *ACS Nano* 6: 7034–7043.
191 O'Connor, T., Panov, M.S., Mereshchenko, A. et al. (2012). *ACS Nano* 6: 8156–8165.
192 Xiang, X., Chou, L., and Li, X. (2013). *Phys. Chem. Chem. Phys.* 15: 19545–19549.
193 Wu, K., Chen, J., McBride, J.R., and Lian, T. (2015). *Science* 349: 632–635.
194 Dana, J., Debnath, T., Maity, P., and Ghosh, H.N. (2015). *J. Phys. Chem. C* 119: 22181–22189.
195 Chauhan, H., Kumar, Y., Dana, J. et al. (2016). *Nanoscale* 8: 15802–15812.
196 Park, G.-S., Kwon, H., Kwak, D.W. et al. (2012). *Nano Lett.* 12: 1638–1642.
197 Su, Y., Wei, X., Peng, F. et al. (2012). *Nano Lett.* 12: 1845–1850.
198 Kang, Z., Yan, X., Zhao, L. et al. *Nano Res.* 2015, 8: 2004–2014.
199 Yu, X., Shavel, A., An, X. et al. (2014). *J. Am. Chem. Soc.* 136: 9236–9239.
200 Dilsaver, P.S., Reichert, M.D., Hallmark, B.L. et al. (2014). *J. Phys. Chem. C* 118: 21226–21234.
201 Sheldon, M.T., Trudeau, P.-E., Mokari, T. et al. (2009). *Nano Lett.* 9: 3676–3682.
202 Xing, M.-Y., Yang, B.-X., Yu, H. et al. (2013). *J. Phys. Chem. Lett.* 4: 3910–3917.
203 Dawson, A. and Kamat, P.V. (2001). *J. Phys. Chem. B* 105: 960–966.

204 Formo, E., Lee, E., Campbell, D., and Xia, Y. (2008). *Nano Lett.* 8: 668–672.
205 Gong, H., Wang, X., Du, Y., and Wang, Q. (2006). *J. Chem. Phys.* 125: 024707.
206 Lee, J.S., Shevchenko, E.V., and Talapin, D.V. (2008). *J. Am. Chem. Soc.* 130: 9673–9675.
207 Kraeutler, B. and Bard, A.J. (1978). *J. Am. Chem. Soc.* 100: 4317–4318.
208 Baba, R., Nakabayashi, S., Fujishima, A., and Kenichi, H. (1985). *J. Phys. Chem.* 89: 1902–1905.
209 Pastoriza-Santos, I., Koktysh, D.S., Mamedov, A.A. et al. (2000). *Langmuir* 16: 2731–2735.
210 Chandrasekharan, N. and Kamat, P.V. (2000). *J. Phys. Chem. B* 104: 10851–10857.
211 Subramanian, V., Wolf, E., and Kamat, P.V. (2001). *J. Phys. Chem. B* 105: 11439–11446.
212 Kamat, P.V. (2002). *J. Phys. Chem. B* 106: 7729–7744.
213 Hirakawa, T. and Kamat, P.V. (2005). *J. Am. Chem. Soc.* 127: 3928–3934.
214 Wood, A., Giersig, M., and Mulvaney, P. (2001). *J. Phys. Chem. B* 105: 8810–8815.
215 Kamat, P.V. (2002). *Pure Appl. Chem.* 74: 1693–1706.
216 Mokari, T., Rothenberg, E., Popov, I. et al. (2004). *Science* 304: 1787–1790.
217 Mokari, T., Sztrum, C.G., Salant, A. et al. (2005). *Nat. Mater.* 14: 855–863.
218 Pacholski, C., Kornowski, A., and Weller, H. (2004). *Angew. Chem. Int. Ed.* 43: 4774–4777.
219 Zheng, Y., Zheng, L., Zhan, Y. et al. (2007). *Inorg. Chem.* 46: 6980–6986.
220 Gu, G., Cheng, C., Huang, H. et al. (2009). *Cryst. Growth Des.* 9: 3278–3285.
221 Fan, F.R., Ding, Y., Liu, D.Y. et al. (2009). *J. Am. Chem. Soc.* 131: 12036–12037.
222 Bian, J.-C., Yang, F., Li, Z. et al. (2012). *Appl. Surf. Sci.* 258: 8548–8551.
223 Mahanti, M. and Basak, D. (2012). *Chem. Phys. Lett.* 542: 110–116.
224 Wang, S., Yu, Y., Zuo, Y. et al. (2012). *Nanoscale* 4: 5895–5901.
225 Xiao, F., Wang, F., Fu, X., and Zheng, Y. (2012). *J. Mater. Chem.* 22: 2868–2877.
226 Geng, J., Song, G.-H., Jia, X.-D. et al. (2012). *J. Phys. Chem. C* 116: 4517–4525.
227 Yu, H., Ming, H., Zhang, H. et al. (2012). *Mater. Chem. Phys.* 137: 113–117.
228 Wang, C., Ranasingha, O., Natesakhawat, S. et al. (2013). *Nanoscale* 5: 6968–6974.
229 Tahir, M.N., Natalio, F., Cambaz, M.A. et al. (2013). *Nanoscale* 5: 9944–9949.
230 Chen, Y., Zeng, D., Zhang, K. et al. (2014). *Nanoscale* 6: 874–881.
231 Zeng, D., Chen, Y., Wang, Z. et al. (2015). *Nanoscale* 7: 11371–11378.
232 Saunders, A.E., Popov, I., and Banin, U. (2006). *J. Phys. Chem. B* 110: 25421–25429.
233 O'Sullivan, C., Ahmed, S., and Ryan, K.M. (2008). *J. Mater. Chem.* 18: 5218–5222.

234 Menagen, G., Mocatta, D., Salant, A. et al. (2008). *Chem. Mater.* 20: 6900–6902.
235 Menagen, G., Macdonald, J.E., Shemesh, Y. et al. (2009). *J. Am. Chem. Soc.* 131: 17406–17411.
236 Khon, E., Hewa-Kasakarage, N.N., Nemitz, I. et al. (2010). *Chem. Mater.* 22: 5929–5936.
237 Chakrabortty, S., Yang, J.A., Tan, Y.M. et al. (2010). *Angew. Chem. Int. Ed.* 49: 2888–2892.
238 Chakrabortty, S., Xing, G., Xu, Y. et al. (2011). *Small* 7: 2847–2852.
239 Li, M., Yu, X.-F., Liang, S. et al. (2011). *Adv. Funct. Mater.* 27: 1–1794.
240 Shanmugapriya, T. and Ramamurthy, P. (2013). *J. Phys. Chem. C* 117: 12272–12278.
241 Han, S., Hu, L., Gao, N. et al. (2014). *Adv. Funct. Mater.* 24: 3725–3733.
242 Kraus-Ophir, S., Ben-Shahar, Y., Banin, U., and Mandler, D. (2014). *Adv. Mater. Interfaces* 1: 1300030.
243 Ha, J.W., Ruberu, T.P.A., Han, R. et al. (2014). *J. Am. Chem. Soc.* 136: 1398–1408.
244 Ben-Shahar, Y., Scotognella, F., Waiskopf, N. et al. (2015). *Small* 11: 462–471.
245 Yu, G., Wang, X., Cao, J. et al. (2016). *Chem. Commun.* 52: 2394–2397.
246 Ben-Shahar, Y., Scotognella, F., Kriegel, I. et al. (2016). *Nat. Commun.* 7: 10413.
247 Waiskopf, N., Ben-Shahar, Y., Galchenko, M. et al. (2016). *Nano Lett* 16: 4266–4273.
248 Aronovitch, E., Kalisman, P., Houben, L., and Bar-Sadan, M. (2016). *Chem. Mater.* 28: 1546–1552.
249 Pawar, A.A., Halivni, S., Waiskopf, N. et al. (2017). *Nano Lett.* 17: 4497–4510.
250 Mokari, T., Aharoni, A., Popov, I., and Banin, U. (2006). *Angew. Chem. Int. Ed.* 45: 8001–8005.
251 Liu, J., Amit, Y., Li, Y. et al. (2016). *Chem. Mater.* 28: 8032–8043.
252 Cozzoli, P.D., Comparelli, R., Fanizza, E. et al. (2004). *J. Am. Chem. Soc.* 126: 3868–3879.
253 Tian, Z., Wang, L., Jia, L. et al. (2013). *RSC Adv.* 3: 6369–6376.
254 Chen, K., Feng, X., Hu, R. et al. (2013). *J. Alloys Compd.* 554: 72–79.
255 Du, P., Cao, Y., Li, D. et al. (2013). *RSC Adv.* 3: 6016–6021.
256 Tanaka, A., Nishino, Y., Sakaguchi, S. et al. (2013). *Chem. Commun.* 49: 2551–2553.
257 Sheng, P., Wu, S., Bao, L. et al. (2012). *New J. Chem.* 36: 2501–2505.
258 Stíbal, D., Sá, J., and von Bokhoven, J.A. (2013). *Catal. Sci. Technol.* 3: 94–98.
259 Wang, P., Dai, W., Ge, L. et al. (2013). *Analyst* 138: 939–945.
260 Zhang, Z., Zhang, L., Hedhili, M.N. et al. (2013). *Nano Lett.* 13: 14–20.
261 Gao, Z.-D., Liu, H.-F., Li, C.-Y., and Song, Y.-Y. (2013). *Chem. Commun.* 49: 774–776.
262 Liu, W.-L., Lin, F.-C., Yang, Y.-C. et al. (2013). *Nanoscale* 5: 7953–7962.
263 Ding, D., Liu, K., He, S. et al. (2014). *Nano Lett* 14: 6731–6736.

264 Goebl, J., Joo, J.B., Dahl, M., and Yin, Y. (2014). *Catal. Today* 225: 90–95.
265 Devadoss, A., Kuragano, A., Terashima, C. et al. (2016). *J. Mater. Chem. B* 4: 220–228.
266 Lee, I., Joo, J.B., Yin, Y., and Zaera, F. (2016). *Surf. Sci.* 648: 150–155.
267 Lee, Y.J., Joo, J.B., Yin, Y., and Zaera, F. (2016). *ACS Energy Lett.* 1: 52–56.
268 Yu, H., Chen, M., Rice, P.M. et al. (2005). *Nano Lett.* 5: 379–382.
269 Shi, W., Zeng, H., Sahoo, Y. et al. (2006). *Nano Lett.* 6: 875–881.
270 Xu, C., Xie, J., Ho, D. et al. (2008). *Angew. Chem. Int. Ed.* 47: 173–176.
271 Shevchenko, E.V., Bodnarchuk, M.I., Kovalenko, M.V. et al. (2008). *Adv. Mater.* 20: 4323–4329.
272 Wu, B., Zhang, H., Chen, C. et al. (2009). *Nano Res.* 2: 975–983.
273 Wang, C., Yin, H., Dai, S., and Sun, S. (2010). *Chem. Mater.* 22: 3277–3282.
274 Zhu, H., Zhu, E., Ou, G. et al. (2010). *Nanoscale Res. Lett.* 5: 1755–1761.
275 Beveridge, J.S., Buck, M.R., Bondi, J.F. et al. (2011). *Angew. Chem. Int. Ed.* 50: 9875–9879.
276 Leung, K.C.-F., Xuan, S., Zhu, X. et al. (2012). *Chem. Soc. Rev.* 41: 1911–1928.
277 Sun, Y., Foley, J.J. IV,, Peng, S. et al. (2013). *Nano Lett.* 13: 3958–3964.
278 Abdulla-Al-Mamun, M., Kusumoto, Y., Zannat, T. et al. (2013). *RSC Adv.* 3: 7816–7827.
279 Liu, S., Gao, S., Sun, S., and You, X.-Z. (2015). *Nanoscale* 7: 4890–4893.
280 Jiang, G., Huang, Y., Zhang, S. et al. (2016). *Nanoscale* 8: 17947–17952.
281 George, C., Genovese, A., Qiao, F. et al. (2011). *Nanoscale* 3: 4647–4654.
282 Khan, G.G., Sarkar, D., Singh, A.K., and Mandal, K. (2013). *RSC Adv.* 3: 1722–1727.
283 Zhang, L., Dou, Y.-H., and Gu, H.-C. (2006). *J. Colloid Interface Sci.* 297: 660–664.
284 Huang, J., Sun, Y., Huang, S. et al. (2011). *J. Mater. Chem.* 21: 17930–17937.
285 Pang, F., Zhang, R., Lan, D., and Ge, J. (2018). *ACS Appl. Mater. Interfaces* 10: 4929–4936.
286 Maaroof, A.I., Cho, D., Kim, B.-J. et al. (2013). *J. Phys. Chem. C* 117: 19601–19605.
287 Schick, I., Lorenz, S., Gehrig, D. et al. (2014). *J. Am. Chem. Soc.* 136: 2473–2483.
288 Zhu, H., Sigdel, A., Zhang, S. et al. (2014). *Angew. Chem. Int. Ed.* 53: 12508–12512.
289 Guo, P., Xu, J., Zhuang, X. et al. (2013). *J. Mater. Chem. C* 1: 566–571.
290 Sheehan, S.W., Noh, H., Brudvig, G.W. et al. (2013). *J. Phys. Chem. C* 117: 927–934.
291 Bai, Y., Zhang, W., Zhang, Z. et al. (2014). *J. Am. Chem. Soc.* 136: 14650–14653.
292 Kuo, C.-H., Hua, T.-E., and Huang, M.H. (2009). *J. Am. Chem. Soc.* 131: 17871–17878.
293 Kuo, C.-H., Yang, Y.-C., Gwo, S., and Huang, M.H. (2011). *J. Am. Chem. Soc.* 133: 1052–1057.
294 Meir, N., Plante, I.J.-L., Flomin, K. et al. (2013). *J. Mater. Chem. A* 1: 1763–1769.

295 Ye, X., Hickey, D.R., Fei, J. et al. (2014). *J. Am. Chem. Soc.* 136: 5106–5115.
296 Nguyen, T.-D., Dinh, C.-T., and Do, T.-O. (2011). *Nanoscale* 3: 1861–1873.
297 Li, Y., Zhang, Q., Nurmikko, A.V., and Sun, S. (2005). *Nano Lett.* 5: 1689–1692.
298 Zhang, X., Tang, A., Jia, Y. et al. (2017). *J. Alloys Compd.* 701: 16–22.
299 Manna, G., Bose, R., and Pradhan, N. (2014). *Angew. Chem. Int. Ed.* 53: 6743–6746.
300 Zhang, J., Tang, Y., Lee, K., and Ouyang, M. (2010). *Science* 327: 1634–1638.
301 Figuerola, A., van Huis, M., Zanella, M. et al. (2010). *Nano Lett.* 10: 3028–3036.
302 Zhao, N., Vickery, J., Guerin, G. et al. (2011). *Angew. Chem. Int. Ed.* 50: 4606–4610.
303 Mishra, N., Lian, J., Chakrabortty, S. et al. (2012). *Chem. Mater.* 24: 2040–2046.
304 Haldar, K.K., Sinha, G., Lahtinen, J., and Patra, A. (2012). *ACS Appl. Mater. Interfaces* 4: 6266–6272.
305 Haldar, K.K., Pradhan, N., and Patra, A. (2013). *Small* 9: 3424–3432.
306 Yu, P., Wen, X., Lee, Y.-C. et al. (2013). *J. Phys. Chem. Lett.* 4: 3596–3601.
307 Das, S., Satpati, B., Chauhan, H. et al. (2014). *RSC Adv.* 4: 64535–64541.
308 Soni, U., Tripathy, P., and Sapra, S. (2014). *J. Phys. Chem. Lett.* 5: 1909–1916.
309 Naskar, S., Schlosser, A., Miethe, J.F. et al. (2015). *Chem. Mater.* 27: 3159–3166.
310 AbouZeid, K.M., Mohamed, M.B., and El-Shall, M.S. (2016). *J. Nanopart. Res.* 18: 8.
311 de la Cueva, L., Meyns, M., Bastús, N.G. et al. (2016). *Chem. Mater.* 28: 2704–2714.
312 Shi, R., Cao, Y., Bao, Y. et al. (2017). *Adv. Mater.* 29: 1700803.
313 O'Sullivan, C., Gunning, R.D., Barrett, C.A. et al. (2010). *J. Mater. Chem.* 20: 7875–7880.
314 Nahar, L., Esteves, R.J.A., Hafiz, S. et al. (2015). *ACS Nano* 9: 9810–9821.
315 Yang, J. and Ying, J.Y. (2009). *Chem. Commun.* 45: 3187–3189.
316 Yang, J. and Ying, J.Y. (2011). *Angew. Chem. Int. Ed.* 50: 4637–4643.
317 Liu, H., Ye, F., Ma, X. et al. (2013). *CrystEngComm* 15: 7740–7747.
318 Pang, M., Hu, J., and Zeng, H.C. (2010). *J. Am. Chem. Soc.* 132: 10771–10785.
319 Liu, B. and Ma, Z. (2011). *Small* 7: 1587–1592.
320 Ma, X., Zhao, Y., Jiang, X. et al. (2012). *ChemPhysChem* 13: 2531–2535.
321 Liu, H., Hu, W., Ye, F. et al. (2013). *RSC Adv.* 3: 616–622.
322 Wang, Z., Liu, J., and Chen, W. (2012). *Dalton Trans.* 41: 4866–4870.
323 Jiang, J., Li, H., and Zhang, L. (2012). *Chem. Eur. J.* 18: 6360–6369.
324 Kim, Y., Park, K.Y., Jang, D.M. et al. (2010). *J. Phys. Chem. C* 114: 22141–22146.
325 Motl, N.E., Bondi, J.E., and Schaak, R.E. (2012). *Chem. Mater.* 24: 1552–1554.
326 Liu, X., Lee, C., Law, W.-C. et al. (2013). *Nano Lett.* 13: 4333–4339.

327 Yang, J., Elim, H.I., Zhang, Q. et al. (2006). *J. Am. Chem. Soc.* 128: 11921–11926.

328 Yang, J., Levina, L., Sargent, E.H., and Kelley, S.O. (2006). *J. Mater. Chem.* 16: 4025–4028.

329 Talapin, D.V., Yu, H., Shevchenko, E.V. et al. (2007). *J. Phys. Chem. C* 111: 14049–14054.

330 Hu, W., Liu, H., Ye, F. et al. (2012). *CrystEngComm* 14: 7049–7054.

331 Franchini, I.R., Bertoni, G., Falqui, A. et al. (2010). *J. Mater. Chem.* 20: 1357–1366.

332 Patra, B.K., Guria, A.K., Dutta, A. et al. (2014). *Chem. Mater.* 26: 7194–7200.

333 Sun, Z., Yang, Z., Zhou, J. et al. (2009). *Angew. Chem. Int. Ed.* 48: 2881–2885.

334 Chen, W.-T. and Hsu, Y.-J. (2010). *Langmuir* 26: 5918–5925.

335 Chen, W.-T., Lin, Y.-K., Yang, T.-T. et al. (2013). *Chem. Commun.* 49: 8486–8488.

336 Du, J., Yu, X., and Di, J. (2013). *J. Solid State Electrochem.* 17: 109–114.

337 Zhu, Y.-F., Zhang, J., Xu, L. et al. (2013). *Phys. Chem. Chem. Phys.* 15: 4041–4048.

338 Bose, R., Wasey, A.H.M.A., Das, G.P., and Pradhan, N. (2014). *J. Phys. Chem. Lett.* 5: 1892–1898.

339 Zhang, Q., Wang, J., Jiang, Z. et al. (2012). *J. Mater. Chem.* 22: 1765–1769.

340 Ha, E., Lee, L.Y.S., Wang, J. et al. (2014). *Adv. Mater.* 26: 3496–3500.

341 Patra, B.K., Shit, A., Guria, A.K. et al. (2015). *Chem. Mater.* 27: 650–657.

342 Sayed, S.Y., Wang, F., Malac, M. et al. (2012). *CrystEngComm* 14: 5230–5234.

343 Ray, M., Basu, T.S., Bandyopadhyay, N.R. et al. (2014). *Nanoscale* 6: 2201–2210.

344 Gu, H., Zheng, R., Zhang, X., and Xu, B. (2004). *J. Am. Chem. Soc.* 126: 5664–5665.

345 Casavola, M., Grillo, V., Carlino, E. et al. (2007). *Nano Lett.* 7: 1386–1395.

346 Elmalem, E., Saunders, A.E., Costi, R. et al. (2008). *Adv. Mater.* 20: 4312–4317.

347 Dukovic, G., Merkle, M.G., Nelson, J.H. et al. (2008). *Adv. Mater.* 20: 4306–4311.

348 Figuerola, A., Fiore, A., Corato, R.D. et al. (2008). *J. Am. Chem. Soc.* 130: 1477–1487.

349 Habas, S.E., Yang, P., and Mokari, T. (2008). *J. Am. Chem. Soc.* 130: 3294–3295.

350 Zhang, H.-T., Ding, J., Chow, G.-M., and Dong, Z.-L. (2008). *Langmur* 24: 13197–13202.

351 Wang, C., Dalmon, H., and Sun, S. (2009). *Nano Lett.* 9: 1493–1496.

352 Deka, S., Falqui, A., Bertoni, G. et al. (2009). *J. Am. Chem. Soc.* 131: 12817–12828.

353 Jen-La Plante, I., Habas, S.E., Yuhas, B.D. et al. (2009). *Chem. Mater.* 21: 3662–3667.

354 Amirav, L. and Alivisatos, A.P. (2010). *J. Phys. Chem. Lett.* 1: 1051–1054.

355 Berr, M., Vaneski, A., Susha, A.S. et al. (2010). *Appl. Phys. Lett.* 97: 093108.
356 Macdonald, J.E., Sadan, M.B., Houben, L. et al. (2010). *Nat. Mater.* 9: 810–815.
357 Shemesh, Y., Macdonald, J.E., Menagen, G., and Banin, U. (2011). *Angew. Chem. Int. Ed.* 50: 1185–1189.
358 Wu, H., Chen, O., Zhuang, J. et al. (2011). *J. Am. Chem. Soc.* 133: 14327–14337.
359 Alemseghed, M.G., Ruberu, T.P.A., and Vela, J. (2011). *Chem. Mater.* 23: 3571–3579.
360 Acharya, K.P., Khnayzer, R.S., O'Connor, T. et al. (2011). *Nano Lett.* 11: 2919–2926.
361 Li, X., Lian, J., Lin, M., and Chan, Y. (2011). *J. Am. Chem. Soc.* 133: 672–675.
362 Berr, M.J., Vaneski, A., Mauser, C. et al. (2012). *Small* 8: 291–297.
363 Buck, M.R., Bondi, J.F., and Schaak, R.E. (2012). *Nat. Chem.* 4: 37–44.
364 Berr, M.J., Wagner, P., Fischbach, S. et al. (2012). *Appl. Phys. Lett.* 100: 223903.
365 Hill, L.J., Bull, M.M., Sung, Y. et al. (2012). *ACS Nano* 6: 8632–8645.
366 Pearson, A., Zheng, H., Kalantar-zadeh, K. et al. (2012). *Langmuir* 28: 14470–14475.
367 Trizio, L.D., Figuerola, A., Manna, L. et al. (2012). *ACS Nano* 6: 32–41.
368 Ding, X., Zou, Y., Ye, F. et al. (2013). *J. Mater. Chem. A* (1): 11880–11886.
369 Schlicke, H., Ghosh, D., Fong, L.-K. et al. (2013). *Angew. Chem. Int. Ed.* 52: 980–982.
370 Liu, H., Ye, F., Cao, H. et al. (2013). *Nanoscale* 5: 6901–6907.
371 Schweinberger, F.F., Berr, M.J., Döblinger, M. et al. (2013). *J. Am. Chem. Soc.* 135: 13262–13265.
372 Siah, W.R., LaGrow, A.P., Banholzer, M.J., and Tilley, R.D. (2013). *Cryst. Growth Des.* 13: 2486–2492.
373 George, C., Genovese, A., Casu, A. et al. (2013). *Nano Lett.* 13: 752–757.
374 Amirav, L. and Alivisatos, A.P. (2013). *J. Am. Chem. Soc.* 135: 13049–13053.
375 Wang, D., Li, X., Li, H. et al. (2013). *J. Mater. Chem. A* 1: 1587–1590.
376 Simon, T., Bouchonville, N., Berr, M.J. et al. (2014). *Nat. Mater.* 13: 1013–1018.
377 Long, R., Mao, K., Gong, M. et al. (2014). *Angew. Chem. Int. Ed.* 53: 3205–3209.
378 Wu, K., Chen, Z., Lv, H. et al. (2014). *J. Am. Chem. Soc.* 136: 7708–7716.
379 Liang, H., Jiang, X., Chen, W. et al. (2014). *Ceram. Int.* 40: 5653–5658.
380 Hodges, J.M., Biacchi, A.J., and Schaak, R.E. (2014). *ACS Nano* 8: 1047–1055.
381 Feng, Y., Liu, H., Wang, P. et al. (2014). *Sci. Rep.* 4: 6204.
382 Bai, S., Ge, J., Wang, L. et al. (2014). *Adv. Mater.* 26: 5689–5695.
383 Liu, H., Ye, F., Cao, H., and Yang, J. (2014). *Nano-Micro Lett.* 6: 252–257.
384 Vinokurov, K., Bekenstein, Y., Gutkin, V. et al. (2014). *CrystEngComm* 16: 9506–9512.
385 Read, C.G., Gordon, T.R., Hodges, J.M., and Schaak, R.E. (2015). *J. Am. Chem. Soc.* 137: 12514–12517.

386 Hodges, J.M., Morse, J.R., Williams, M.E., and Schaak, R.E. (2015). *J. Am. Chem. Soc.* 137: 15493–15500.

387 Oshima, T., Lu, D., Ishitani, O., and Maeda, K. (2015). *Angew. Chem. Int. Ed.* 54: 2698–2702.

388 Sung, Y., Lim, J., Koh, J.H. et al. (2015). *CrystEngComm* 17: 8423–8427.

389 Bradley, M.J., Read, C.G., and Schaak, R.E. (2015). *J. Phys. Chem. C* 119: 8952–8959.

390 Hernández-Pagán, E.A., Leach, A.D.P., Rhodes, J.M. et al. (2015). *Chem. Mater.* 27: 7969–7976.

391 Aronovitch, E., Kalisman, P., Mangel, S. et al. (2015). *J. Phys. Chem. Lett.* 6: 3760–3764.

392 Amirav, L., Oba, F., Aloni, S., and Alivisatos, A.P. (2015). *Angew. Chem. Int. Ed.* 54: 1–6.

393 Chowdhury, P., Gomaa, H., and Ray, A.K. (2015). *Chemosphere* 121: 54–61.

394 Bai, S., Yang, L., Wang, C. et al. (2015). *Angew. Chem. Int. Ed.* 54: 14810–14814.

395 Kalisman, P., Houben, L., Aronovitch, E. et al. (2015). *J. Mater. Chem. A* 3: 19679–19682.

396 Kalisman, P., Kauffmann, Y., and Amirav, L. (2015). *J. Mater. Chem. A* 3: 3261–3265.

397 Chen, D., Liu, H., Cui, P. et al. (2015). *CrystEngComm* 17: 6155–6162.

398 Chen, D., Cui, P., Liu, H., and Yang, J. (2015). *Electrochim. Acta* 153: 461–467.

399 Feng, J., An, C., Dai, L. et al. (2016). *Chem. Eng. J.* 283: 351–357.

400 Bai, Y., Wang, C., Zhou, X. et al. (2016). *Prog. Nat. Sci.* 26: 289–294.

401 Li, R., Wu, S., Wan, X. et al. (2016). *Inorg. Chem. Front.* 3: 104–110.

402 Bai, S., Xie, M., Kong, Q. et al. (2016). *Part. Part. Syst. Charact.* 33: 506–511.

403 Grabowska, E., Marchelek, M., Klimczuk, T. et al. (2016). *J. Mol. Catal. A: Chem.* 423: 191–206.

404 Kalisman, P., Nakibli, Y., and Amirav, L. (2016). *Nano Lett.* 16: 1776–1781.

405 Cui, P., He, H., Liu, H. et al. (2016). *J. Power Sources* 327: 432–437.

406 Zhu, Y., Gao, C., Bai, S. et al. (2017). *Nano Res.* 10: 3396–3406.

407 Jin, J., Wang, C., Ren, X.-N. et al. (2017). *Nano Energy* 38: 118–126.

408 Li, M., Zhang, N., Long, R. et al. (2017). *Small* 13: 1604173.

409 Yang, W., Yu, Y., Tang, Y. et al. (2017). *Nanoscale* 9: 1022–1027.

410 Cherukara, M.J., Sasikumar, K., DiChiara, A. et al. (2017). *Nano Lett.* 17: 7696–7701.

411 Tang, J., Chen, D., Li, C. et al. (2017). *RSC Adv.* 7: 3455–3460.

412 Choi, J.Y., Jeong, D., Lee, S.J. et al. (2017). *Nano Lett.* 17: 5688–5694.

413 Lamer, V.K. and Dinegar, R.H. (1950). *J. Am. Chem. Soc.* 72: 4847–4854.

414 Nasilowski, M., Mahler, B., Lhuillier, E. et al. (2016). *Chem. Rev.* 116: 10934–10982.

415 Peng, X., Wickham, J., and Alivisatos, A.P. (1998). *J. Am. Chem. Soc.* 120: 5343–5344.

416 Peng, Z. and Peng, X. (2002). *J. Am. Chem. Soc.* 124: 3343–3353.

417 Jana, N.R., Gearheart, L., and Murphy, C.J. (2001). *Chem. Mater* 13: 2313–2322.

418 Yu, H., Gibbons, P.C., Kelton, K.F., and Buhro, W.E. (2001). *J. Am. Chem. Soc.* 123: 9198–9199.

419 Wilcoxon, J.P. and Provencio, P.P. (2004). *J. Am. Chem. Soc.* 126: 6402–6408.

420 Park, J., Lee, E., Hwang, N.M. et al. (2005). *Angew. Chem. Int. Ed.* 44: 2872–2877.

421 Tao, A.R., Habas, S., and Yang, P. (2008). *Small* 4: 310–325.

422 Murray, C.B., Norris, D.J., and Bawendi, M.G. (1993). *J. Am. Chem. Soc.* 115: 8706–8715.

423 Talapin, D.V., Rogach, A.L., Shevchenko, E.V. et al. (2002). *J. Am. Chem. Soc.* 124: 5782–5790.

424 Hambrock, J., Becker, R., Birkner, A. et al. (2002). *Chem. Commun.* 68–69.

425 Jana, N.R. and Peng, X. (2003). *J. Am. Chem. Soc.* 125: 14280–14281.

426 Prasad, B.L.V., Stoeva, S.I., Sorensen, C.M., and Klabunde, K.J. (2003). *Chem. Mater.* 15: 935–942.

427 Kim, S.-W., Park, J., Jang, Y. et al. (2003). *Nano Lett.* 3: 1289–1291.

428 Jun, Y., Choi, J., and Cheon, J. (2006). *Angew. Chem. Int. Ed.* 45: 3414–3439.

429 Park, J., Joo, J., Kwon, S.G. et al. (2007). *Angew. Chem. Int. Ed.* 46: 4630–4660.

430 Sidhaye, D.S. and Prasad, B.L.V. (2011). *New J. Chem.* 35: 755–763.

431 Mullin, J.W. (1997). *Crystallization*, 3e. Oxford: Butterworth-Heinemann.

432 Sugimoto, T. (2001). *Monodisperse Particles*. Amsterdam: Elsevier.

433 Markov, I.V. (2003). *Crystal Growth for Beginners: Fundamentals of Nucleation, Crystal Growth, and Epitaxy*. Singapore: World Scientific.

434 Cozzoli, P.D. (ed.) (2008). *Advanced Wet-Chemical Synthetic Approaches to Inorganic Nanostructures*. Kerala, India: Transworld Research Network.

435 Yang, J. and Ying, J.Y. (2010). *J. Am. Chem. Soc.* 132: 2114–2115.